University of Alberta

A molecular dynamics simulation study on Bauschinger's effect in nano-scaled Cu systems with and without interfaces

by

Di Zhu

A thesis submitted to the Faculty of Graduate Studies and Research
in partial fulfillment of the requirements for the degree of

Master of Science

in

Materials Engineering

Department of Chemical and Materials Engineering

Spring 2013
Edmonton, Alberta

Abstract

Employing the molecular dynamics simulation method, we investigated the responses of nano-scaled Cu systems, including single crystal(SC), and crystals with twin boundaries(TW) and grain boundaries(GB) to cyclic deformation in different strain ranges. Bauschinger's effect occurring during the cyclic processes was quantified, which showed a decreasing trend in the sequence of SC, GB and TW. The simulation results show that in the nano-scaled systems the annihilation of partial dislocations with opposite signs and shrinkage of associated stacking faults could be more responsible for the Bauchinger's effect due to the narrowed spacing between boundaries, which may confine reversible movement of generated dislocations. The suggestion is supported by changes in some crucial parameters during cyclic loading processes, such as fluctuations of absorbed strain energy, variations in the amount of defect atoms, failure strains and stress concentrations before fracture. Efforts are made to elucidate possible mechanisms responsible for the observed phenomena.

Acknowledgements

I'd like to extend my genuine gratitude to my supervisor Dr. Dongyang Li and co-supervisor Dr. Hao Zhang who offered me the opportunity to pursue my master degree at University of Alberta. I have owed them so much in the more than two years' study that the words "thank you" are not even close to expressing my admiration. They do not only teach me how to observe the underlying principles from the phenomena, but also help me to open new insights into various approaches to deal with all kinds of problems. Under their professional guidance, I can gradually develop my academic background in a much more appropriate way than usual, both literarily and orally.

I also appreciate the supports from all my colleagues, who helped me a lot and gave me useful advices with their own experience in facing difficulties.

Table of Contents

List of Tables

List of Figures

Chapter 1 Introduction

1.1 What is Bauschinger's effect?

Bauschinger effect was first noticed and described by the German engineer, Johann Bauschinger, more than one century ago, which refers to the phenomenon that a pre-deformed metal plastically shows a lower yield strength when the applied stress is reversed, as illustrated in Fig.1.1. According to the theory of plasticity, the Bauschinger's effect reflects effects of both the history of cold working and current stress distribution on forward and reverse loading flow behavior of a metal [1]. Considerable effort has been dedicated by many researchers to understand the Bauschinger's effect, which is of importance to the performance of materials during cyclic loading processes such as fatigue [2] and wear [4, 7] through changing the defect pile-up and consequently the stress concentrations. There have been many studies on Bauschinger's effect reported in the literature, including experimental investigations[3-7] and computational studies [8-16] in order to take advantage of this effect to optimize the performance of materials, e.g., improving the machining efficiency or maximizing the resistance of materials to wear. For instance, Jordon et al. [3] tested rolled and cast aluminum alloys on different prestrain levels in tension and compression, and showed that

damage nucleation rate can be altered due to the Bauschinger's effect.

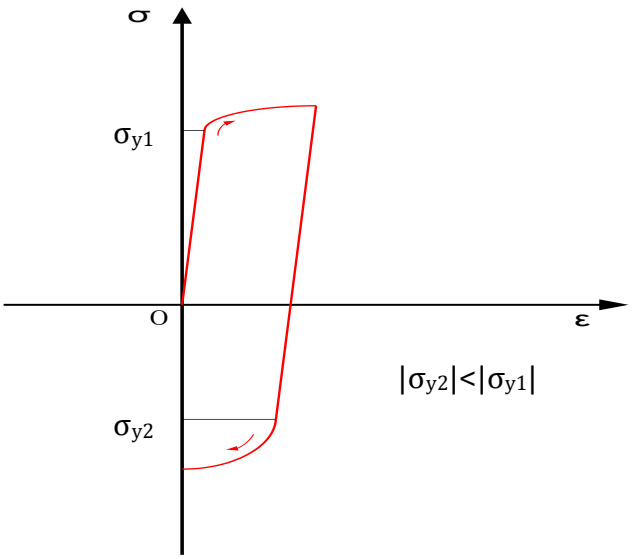

Fig.1.1 A Schematic representation of Bauschinger's effect of metals during tension-compression tests. After plastically deformed in tension, the yield strength, $|\sigma_{y2}|$, is lower than $|\sigma_{y1}|$ when the stress is reversed.

1.2 The loading-path dependence of Bauschinger's effect and its significance to industry

Bauschinger's effect certainly plays a role in failure of materials as the deformation is loading-path dependent. Lukas et al. [17] investigated stress-strain response and fatigue life of copper single crystals cyclically loaded with a positive mean stress, and demonstrated that the corresponding dislocation structure had a homogeneous cell structure lying mainly along the primary slip plane and gradually formed the surface slip markings and

microcracks. Kiener et al. [18] performed in-situ miniaturized bending fatigue tests for copper single crystals and observed remarkable monotonic hardening behavior and enlarged Bauschinger's effect with increasing normalized displacement. Chawla et al. [19] examined a porous sintered Fe-Mo steel under tension-compression and vice-versa, and observed a stronger Bauschinger's effect in the latter process, compared to the former. Demir and Raabe [20] studied Bauschinger's effect in single-crystal copper and suggested that Bauschinger's effect involved two processes denoted as "mechanical Bauschinger effect" which referred to a yield stress drop and the "microstructural Bauschinger effect" which described the degree of microstructure reversibility with changed loading paths.

As a result of Bauschinger's effect, the effectiveness of bi-directional machining is different from that of unidirectional machining due to the Bauschinger's effect. By designing an appropriate machining process and optimal geometry of cutting tool, one could maximize the machining efficiency and reduce related energy consumption. For instance, Tang et al. [9] investigated wear losses of Cu-40%Zn alloy caused by a steel counter-face during unidirectional abrasion and bidirectional abrasion processes, respectively. They observed that the former caused more wear than the latter and demonstrated that this difference in wear was attributed to Bauschinger's

effect, which affected the strain-hardening and thus the failure behavior.

These studies have confirmed the dependence of Bauschinger's effect on the loading path. However, to what extend the Bauschinger's effect depends, what happens locally inside the materials and how the local events are related to the unique performance of the materials still need to be answered.

1.3 Mechanisms responsible for Bauschinger effect's

Possible mechanisms for Bauschinger's effect are generally classified into two groups: 1) long range stresses or back stresses, originated from the dislocation pile-ups at interfaces, may drive dislocations move backwards, thus lowering the yield strength in the opposite direction; 2) cancelation of generated dislocations with opposite signs when external stress was reversed [21]. Bauschinger's effect is influenced by many other factors. For instance, Stoltz and Pelloux [21] investigated the difference in Bauschinger's effect between precipitation-strengthened Al alloys with nonshearable particles and shearable particles and found extraordinary Bauschinger's effect in the alloy with nonshearable precipitates. Based on electron micrographs of all samples, they suggested that the Bauchinger's effect at small strains in alloys with unshearable precipitates was primarily due to internal long range stress or back stress origin from the tangling or interactions of dislocations with the

particles. Moan and Embury [22] also performed tension-compression tests to investigate the strain hardening in Al-Cu alloys aged to nonshearable participation conditions; their results showed that at small strains, the magnitude of back stress depended on dislocation loops accumulated around either individual particles or groups of them, while at large strains, the value of back stress partly lowered regarding to cutting of particles by matrix dislocations. In the meantime, introduction of double or multiple slip systems reduced the back stress due to the formation of prismatic loops in contrast to single slip orientations. In order to take insight into internal stress status and stored energy gained during straining, Pedersen et al [5] proposed a long range internal stresses model to explain Bauschinger's behavior in work-hardened copper in comparison with that of a composite. Bate and Wilson [23] discussed the relationship between internal stress and Bauschinger's effect in some inhomogeneous material under monotonic and reversed processing conditions. Most explanations for Bauschinger's effect in macro-scale metals were based on the long-range stress mechanism. However, the information on local Bauschinger's effect especially in nanostructured materials is rather limited.

In order to obtain more information on Bauschinger's effect, considerable modeling studies have also been conducted. Bauschinger's effect is influenced

by many factors such as grain boundaries, twinning, inter-phase boundaries and second phases etc. Setoodeh and Attariani [24] reported the existence of Bauschinger's effect in infinite nickel nanowire based on implement of tension-compression test at a strain rate of 0.86% ps^{-1} at room temperature and a molecular dynamics simulation study. Two phenomena were observed in their tests: 1) the stress-strain curves had saw-shape portions which were attributed to various dislocation activities, like nucleation, annihilation and junction etc.; and 2) the Bauschinger effect in nickel nanowire was enlarged with the increment of prestrain. HSU and Arsenault [25] reported reduction of Bauschinger's effect (BE) in copper single crystals during alternate tension and compression tests and suggested that: 1) dislocation movements were commanded by thermodynamic driven jumps over short-range barriers; 2) it needed a lower stress to trigger dislocation surface sources than that in the internal sources. Their dislocation model describes a surface with high density of inversely pile-up dislocations, and each dislocation has to jump over a short-range barrier to move forward beyond necessary driven force. Regarding the reverse loading process, new features were added to the model. Firstly, consideration of new slip planes activated in reverse straining led to an "alternate-plane mode" which consisted of alternative arrangement of slip planes with only positive or negative sign of dislocations in each plane

regardless of any interactions between the neighbors. Secondly, given the newly nucleated dislocations with opposite sign to the original ones existing on the same plane during reverse loading, a "coplanar mode" was included. In this mode, the cancellation of dislocations with different signs happens on the same slip systems until the original positive dislocations are exhausted.

1.4 Effect of Microstructure on Bauschinger's effect

The mechanical behavior of a realistic material is largely affected by microstructural factors such as the interface between participates and matrix, grain boundaries, twin boundaries and so on. Mechanical properties of a metal are closely connected with structure and distributions of its dislocations. This study is conducted to investigate Bauschinger's effect in copper, a FCC metal. For FCC metals, their deformation is achieved by both dislocation movement and stacking faults. As shown in Fig.1.2, a normal stacking sequence of the neighboring closed-packed FCC lattices is CBACBAC…. When a {111} plane (i.e. C plane) is removed, the original stacking sequence changes to CBABAC…, where a stacking fault is produced between the red letters, which is named "intrinsic stacking". We may also produce a stacking fault by inserting a disc of clustered interstitials (i.e. B plane), compared to the agglomerated vacancies on a plane, and the stacking sequence is changed to CBABCBAC…, which is called an "extrinsic stacking fault". In both situations, dislocations are

simultaneously generated adjacent to the produced stacking fault, whose movement leads to the extension or shrinkage of the stacking fault. The direction of these dislocations is described by the Burgers vector $\mathbf{b}=\pm\mathbf{a}/3<111>$ and called partial dislocations or Frank dislocations, where **a** represents the unit vector of the lattice.

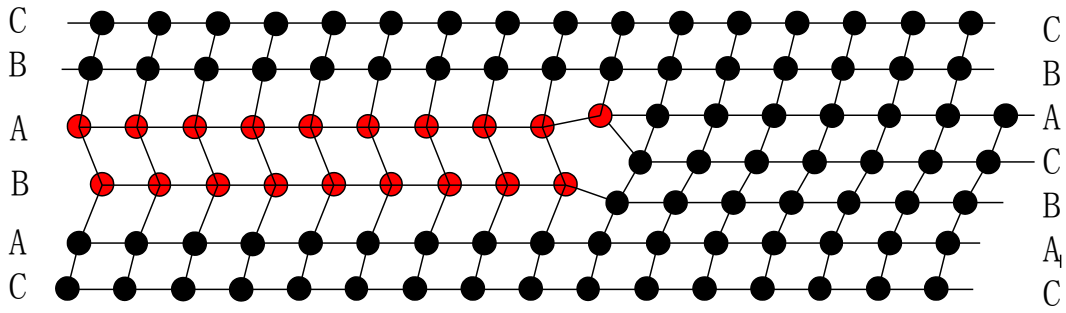

(a) Intrinsic stacking fault

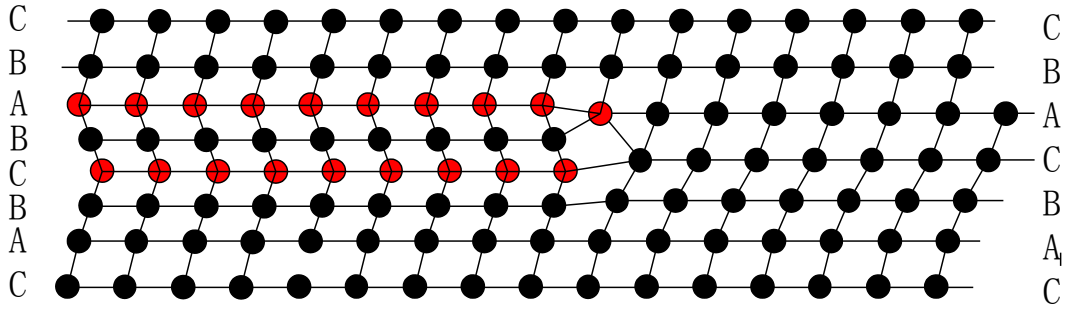

(b) Extrinsic stacking fault

Fig.1.2 A representation of two types of stacking faults in a FCC metal:(a) Intrinsic stacking fault;(b) Extrinsic stacking fault.

In many FCC metals such as copper, particularly in nanoscale crystal, the

deformation at room temperature is achieved by generation of stacking faults and the movement of partial dislocations associated with the stacking faults [26] as well as the formation of others such as dislocation cells [27, 28]. The extension/shrinkage of the stacking faults and associated dislocation movement play roles in the Bauschinger's effect. Any obstacle to their movement could influence the Bauschinger's effect.

1.4.1 Twin boundaries in FCC crystals

Twin boundaries, as illustrated in Fig.1.3, certainly affect the mechanical behavior of Cu and thus the Bauschinger's effect. It has been demonstrated

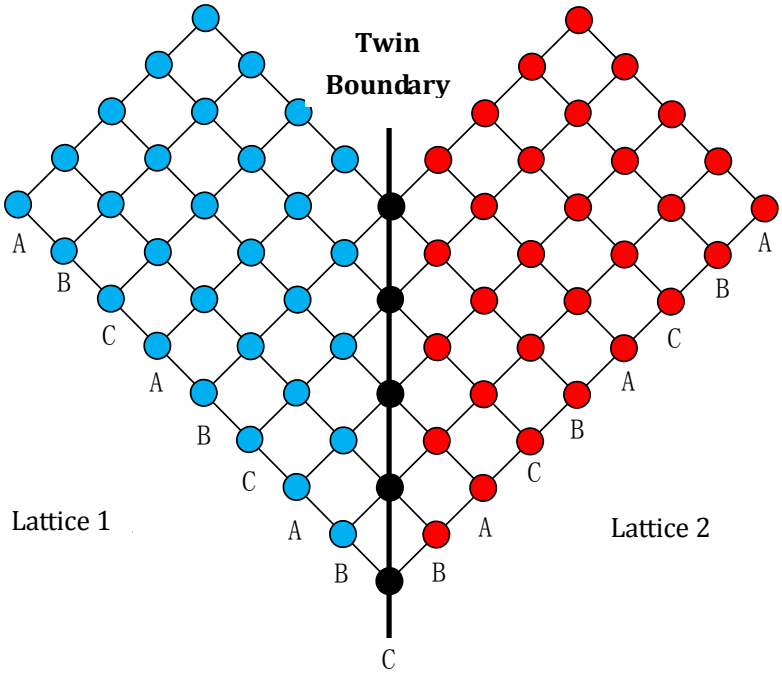

Fig.1.3 A scheme of twin boundary in a FCC metal

that twin boundaries (TWs) are beneficial to some mechanical behavior of

copper. Shute et al [29] studied effects of stress-controlled tension-tension cyclic deformation and severe compression tests on as-deposited Cu/Cu multilayer samples with nanoscale twinning. They observed that nano-twined copper had higher stability with considerably increased fatigue life and hardness, compared to copper with coarse grains. Lu et al [30] reported that nanometer-sized twinning developed in copper deposits exhibited prominent increment in strength with decreasing twin boundary spacing while retaining desired ductility. The benefits from the twinning could be attributed to the ordered twin boundaries, which effectively block dislocation movement with low dislocation emission. Dao et al [31] reported the enhancement in strength, strain-rate sensitivity and ductility of copper with decreasing the twin boundary spacing. They suggested that the dislocation activities in the vicinity of twin boundaries played a crucial role in plastic deformation for the nano-twinned copper, and considerable plastic anisotropy could be expected with relatively easy shear deformation parallel to TWs (soft mode) and difficult shear deformation across the TWs (hard mode). Using a discrete twin crystal plasticity (DT-CP) model, Mirkhani and Joshi [32] investigated the plastic deformation for the transition in yield strength of nano-twinned Cu from strengthening to softening, as the twin spacing decreased and suggested that this yield response might be ascribed to the competition between the

anisotropic strengthening due to dislocation pile-up at TW boundaries and the softening associated with the source-governed dislocation nucleation and successively additional slip in twin-boundary-affected-zone (TBAZ). Shabib and Miller [33] conducted a MD simulation study on twinning in copper and demonstrated that the toughness of nano-twinned Cu was increased with a decrease in the twin width and at very low temperature, which was largely contributed to the free dislocation motion along TWs, while grain size refinement decreased the toughness. Marchenko and Zhang [34] studied the effect of twin boundary spacing with fixed TWs' density as well as the grain size on the deformation behavior of nano-twinned columnar-grained copper during tensile loading. They observed that both twin boundary/grain boundary (TW/GB) distance and grain size refinement could be positively related to the enhancement in strength, toughness and work hardening in nanocrystalline twinning metals. This phenomenon could be attributed to GB-mediated emission of partial dislocations from grain boundaries and grain boundary sliding. By characterize the Bauschinger stress in large offset shear strain of 5%, Stout and Rollett [35] attributed the samples' mechanical behavior to isotropic hardening combined with different structures of generated dislocations, regardless of the long range internal stresses built up in the interface between incoherent particles and matrix, which are largely

limited by the relaxation developing in the matrix. The mechanism of Bauschinger's effect could thus be related to the dislocation substructures: 1) for materials that form series of dislocation cells and subgrains, like Oxygen free copper (OFE copper) and pure Al, Bauschinger effect is accounted for the untangling of dislocation cell substructure that began at some critical yield stress, whose stability is a monotonic function of stacking fault energy. Lowering the stacking fault energy will develop a microband, a more stable microstructure than an equiaxed cell, which can act as channels for dislocation motion; 2) for materials with low stacking fault energy and planar slip systems, Bauschinger effect could be contributed by portions of intersecting dislocations which act as permeable barriers to dislocation movement, driven by a few dislocation pile-ups. Thus, as the stress is reversed, secondary slip system is activated and the stress level rises rapidly to be equal or even over the previous stress in the forward region, resulting in a higher rate of dislocation nucleation in the newly triggered slip plane than that in the monotonic deformation; 3) for planar deformed materials with twin boundaries, permanent softening and strong Bauschinger effect is observed, which results from the blocking of the hard barriers on dislocation movement. As these obstacles can support large amount of planar pileups of generated dislocations, the materials may yield at a much lower stress when the straining

direction is reversed and the blocking effect of these barriers to dislocation motion is substantially lowered. Karaman et al [36] performed forward compression/reverse tension(FC/RT) and forward tension/reverse compression(FT/RC) tests at a strain rate of $5X10^{-5}s^{-1}$ respectively for Hadfield steel single crystals along three crystalline orientations, [$\bar{1}$11], [$\bar{1}$23] and [001], to investigate two competitive but interactive mechanisms, deformation twinning and slipping, for Bauschinger effect. The twin boundaries and localized slip boundaries, such as macro-shear-bands (MSBs) and dislocation tangles, may act as hard but penetrable obstacles, where a long range internal stress could be built up and accumulated. Whenever twinning is the onset mechanism of deformation, and generated partial dislocations piled up at the twin boundaries and gained sufficient back stresses, a large drop of strength may occur when the applied stress is reversed and thus leads to softening and significant Bauschinger effect, like the forward compression/reverse tension case in samples of [001] orientation. Dislocations can also pile up at macro-shear-bands and provide back stress to aid the dislocations to move backwards, but the generated back stress here is not remarkable, compared to that built up in front of twin boundaries, indicating that twin boundaries are stronger barriers than localized slip bands. This theory is justified by the forward compression/reverse tension

experiment of samples with [$\bar{1}11$] and [$\bar{1}23$] orientations, which display a transient region without appreciable permanent softening when the loading direction is reversed, when macro-shear-bands controll the reversed deformation.

Thus, twin boundaries may enhance Bauschinger's effect, since they act as barriers to deformation. When the applied stress is reversed, it is easier for large quantities of generated partial dislocations and stacking faults moved backward and relax the local stress built up in front of the twin boundaries. However, if it may not be the same story in nano-scale copper crystals containing coherent twin boundaries with extremely small spacing, e.g., 10nm, between the twin boundaries.

1.4.2 Grain Boundaries in FCC crystals

Disordered grain boundary, as shown in Fig.1.4, also influences Bauschinger's effect. In polycrystalline materials, Bauschinger's effect is affected by grain boundaries [37], which develop residual stresses. The presence of grain boundaries may favor Bauschinger's effect, since they could enhance nucleation of slip bands where dislocations move backwards when the applied stress is reversed [38-40]. Yaguchi and Margolin [41] studied the contribution of grain boundaries to Bauschinger's effect in β-brass bicrystals under cyclic straining. They observed that Bauschinger effect increased with

increasing the volume fraction of grain boudnaries and increment of strain. They also reported that the Bauschinger effect was stronger undergoing compression-tension than the opposite loading sequence.

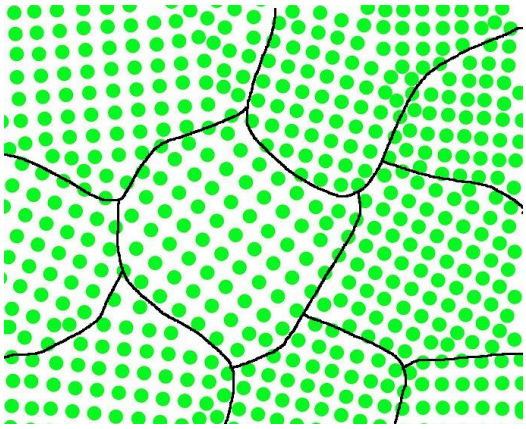

Fig.1.4 A schematic representation of grain boundaries in polycrystalline material

For polycrystalline materials, Bauschinger's effect has been extensively investigated [42-47]. It is generally accepted that grain boundaries enhance the Bauschinger's effect by increasing the back stress created by dislocation pile-ups in front of grain boundaries. Danilov [48] demonstrated that the Bauschinger effect is weakened with increasing grain size in polycrystalline copper, indicating that grain boundaries promoted the Bauschinger's effect. Yaguchi and Margolin [49] showed that the Bauschinger stress in brass bicrystals was larger than that in single crystals. Recently studies include grain boundaries' effects on various aspects, such as energy variations in different FCC crystals [50], diffusion induced migration in bisystem [51, 52], and effect

of grain boundary on variations in the saturation stress during cyclic loading processes [53]. Computer modeling studies also generate consistent information. Using MD simulation, Fang et al [54] investigated Bauschinger's effect in nickel single crystals and nickel containing arrays of high-angle and low-angle grain boundaries, and demonstrated that the Bauschinger effect was the largest with the high angle boundaries and the lowest for the single crystal. The low-angle grain boundaries show a weaker capability to block dislocation movement, since grain boundaries with low misorientations do not generate a large barrier to dislocations.

However, the obtained information is still limited, especially on the Bauschinger's effect in nanocrystalline materials, in which the number of dislocations and their length are largely limited by the nano-sized grains. The internal stress fields caused by grain boundaries could be mutually interfered due to the small spacing between the boundaries, which may thus influence the dislocation pile-up. Vinogradov et al [55] investigated the response of ultrafine- grained (UFG) copper of 200 nm in average grain size to cyclic loading, in comparison with that of coarse-grained (CG) copper; they observed significant difference in fatigue behavior between UFG and CG samples and that there was no much strain localization in the UFG. The CG sample showed a larger Bauschinger energy parameter corresponding to

stronger Bauschinger's effect. Tagarielli et al [56] investigated the mechanical behavior of nanocrystalline Fe/Cu composites and noticed that the composites displayed negligible strain hardening and a symmetric response in tension and compression, which is an indication of negligible Bauschinger's effect. The defect activities in nano-scaled copper systems and the emission of defects from grain boundaries with ease in the nano-scaled copper systems should partially correspond to the inverse Petch-Hall effect in nanocrystalline materials when the grain size is reduced to the range of 10 nm [57].

1.5 Summary

Plastic deformation in copper crystals involves generation and propagation of partial dislocations, which may jump, tangle, slide, and interact with other produced defects and are of importance to shrinkage or extension of stacking faults and material failure. These processes are largely alternated by cyclic loading, which may be related to Bauschinger's effect, a well-known phenomenon. A metal may become softer with lower yield strength when pre-strained in opposite direction. The Bauschinger's effect is of significance to industrial application and technical advances and can be remarkably affected by microstructure of materials. Great efforts have been

made to understand the influence of microstructure and imperfections on the Bauschinger's effect in the FCC metals during deformation. It has been demonstrated that twin boundaries and grain boundaries may enhance the Bauschinger's effect in copper crystalline compared to that in Cu single crystals. However, the situation could be different for nanocrystalline materials and relevant knowledge is very limited. It is worthy studying the effect of twin boundaries and grain boundaries on Bauschinger's effect in nano-scale copper systems in order to take advantage of Bauschinger's effect in nanocrystalline materials.

The objectives in this study are:

(1) to computationally investigate Bauschinger's effect in single crystal copper subjected to cyclic loading;

(2) to investigate the influence of nano-twin boundaries in copper on the Bauschinger's effect and variations in relevant parameters, including the defect quantities, strain energy and failure strain, which are related to the Bauschinger's effect;

(3) to investigate the influence of grain boundaries in nano-Cu systems on Bauschigner's effect, in comparison with those in single crystal and one containing twin boundaries on nano-scale.

The studies for achieving the above three objectives are reported in

chapters three, four and five, respectively.

Chapter 2 Simulation Methodology

In this chapter, the methodology used in the simulation study is described, including molecular dynamics method, specific procedures and arrangments for this study, and relevant technical issues.

2.1 Introduction to Computer Simulation

Computer simulation has emerged and acted as an effective and supplementary approach to experimental and theoretical techniques in scientific and engineering studies. Due to various limitations, experimental studies may not be able to reveal roles of different parameters in a specific process. However, such limitations may not exist for computer simulation. "Computational experiments" could be arranged under controllable conditions so that detailed information about a process could be obtained and roles of individual factors in the process could be studied separately.

2.2 Molecular Dynamics Simulation

An important technique in computer simulation is the Molecular Dynamics (MD). In a MD system consisting of interacting atoms, a process is described by determining trajectory and movement of individual atoms based on

Newton's law of motion. In molecular dynamics simulation, we follow the laws of classical mechanics, mainly the Newton's Law: $\boldsymbol{F}_i=m_i\boldsymbol{a}_i$, where m_i is the mass of atom i in a system containing N atoms, $\boldsymbol{a}_i$ is its acceleration and $\boldsymbol{F}_i$ is the force on atom i which is the sum of interactions between this atom and other atoms in the system. After setting up initial conditions - initial positions and velocities of all atoms in the system, the following microstructure evolution can be simulated based on Newton's Law. Corresponding equilibrium properties can also be predicted [58].

2.3 Model Construction and Operation

In the present study, the modeling was carried out for three Cu systems, including single crystal (SC), crystals with grain boundaries (GB) and twin boundaries (TW), respectively. Each of the systems consisted of 58775~58799 atoms with a dimension of 20.7 x 9.34 x 3.6nm and had its [111], $[1\bar{1}0]$ and $[11\bar{2}]$ crystallographic orientations parallel to X, Y and Z axes, respectively, as illustrated in Fig.2.1. The TW system had two Σ3 coherent boundaries with a spacing of 10nm, and one atom was removed from the center of both the system to guarantee plastic deformation initiating at the center instead of the edges. We also removed one atom from the center of the SC system to keep the same condition. For the GB system, it had two Σ7 tilt

boundaries with a misorientation angle of 38.5°and 1% vacancies were introduced to increase grain boundary energy or reduce its density. The spacing between the two grain boundaries was 10nm.

Three layers of atoms at both ends of each system were fixed and an external displacement was applied along the X axis under a strain rate of $10^{7}s^{-1}$. Periodical boundary conditions were applied to both Y and Z directions, along which the applied stress was set to be zero. The systems were relaxed and achieved thermodynamic equilibrium under 300K for 500ps using NVT ensemble through the Nose-Hoover thermostat [59, 60]. After the relaxation, some vacancies may diffuse from the grain boundaries in the GB system into the middle of the model. Besides, the embedded-atom method (EAM) determined potential in Mishin's form [61, 62] for Cu were used here as the constitutive law for atomic interactions.

(a)

(b)

(c)

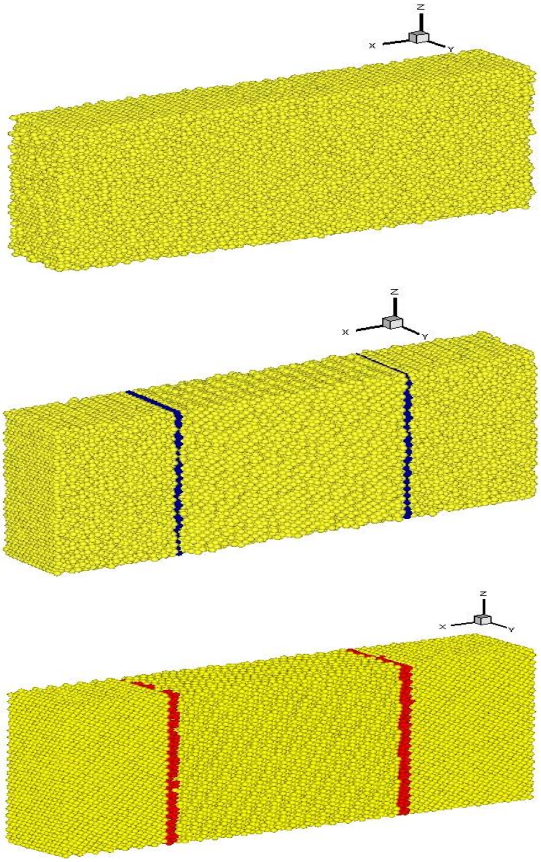

Fig.2.1 The scheme of three nano-Cu crystal models with their [111], [1$\bar{1}$0] and [11$\bar{2}$] crystallographic orientations respectively parallel to X, Y and Z axes: (a) a SC system; (b) a TW system having two Σ3 coherent twin boundaries with a spacing of 10 nm; (c) a GB system having two Σ7 grain boundaries with a spacing of 10 nm and 1% vacancies in the grain boundaries. Yellow atoms in all three models indicate the FCC atoms; Blue atoms in the TW model represent two Σ3 coherent twin boundaries; and red atoms in the GB model display two Σ7 grain boundaries.

Using LAMMPS [63] software, deformation of each system was simulated under cyclic tension-compression applied in the X direction at the room temperature using NPT ensemble in the Nose-Hoover thermostat. Three strain

ranges of $\pm 10\%$, $\pm 15\%$ and $\pm 20\%$ were used for the simulation. All systems were first pulled to the maximum strain, i.e. 10% for example, and then the cyclic loading process began with symmetrically successive compression. After nine cycles, the samples were pulled to failure.

To identify the local crystal structure around each atom in the selected group, the Common Neighbor Analysis (CNA) method [64] was employed. With this approach, one can distinguish atomistic configurations between crystal defects, like stacking faults (HCP atoms), partial dislocations as well as clusters of vacancies, and perfect crystal, like FCC.

Chapter 3 Bauschinger's effect in deformed copper single crystal

Plastic pre-strain may decrease the yield strength of metallic materials when stressed in the opposite direction, known as Bauschinger's effect, which could considerably influence the performance of the materials. However, various processes on microscopic level associated with the Bauschinger's effect are still not clear. In part of this study, defect generation, movement and annihilation in single crystal copper during cyclic tension-compression loading processes were simulated using the molecular dynamics method. It was observed that Bauschinger's effect was asymmetrical and the strain hardening was more profound during compression. After plastic compression, the tensile fracture strain was increased. The absorbed energy was self-adjusted during the tension-compression cycles and kept relatively stable during the loading cycles. In this chapter, the observed phenomena are reported and the mechanisms responsible for these phenomena are discussed.

3.1 Loading Procedure

After thermal equilibration, three identical copper single crystal systems were deformed by cyclic tension-compression respectively in three different

strain ranges along the X axis parallel to the [111] crystallographic direction, with a loading rate equal to $10^7 s^{-1}$. Each system was first pulled to the maximum tensile value, and then the cyclic process was started with compression. After nine cyclic loading cycles, all the samples were pulled to failure to see how the compression-tension cycles affected the failure strain. Fig.3.1 illustrates a model system subjected to cyclic deformation in the strain range of $\pm 10\%$. After nine cycles, the sample was pulled up to fracture.

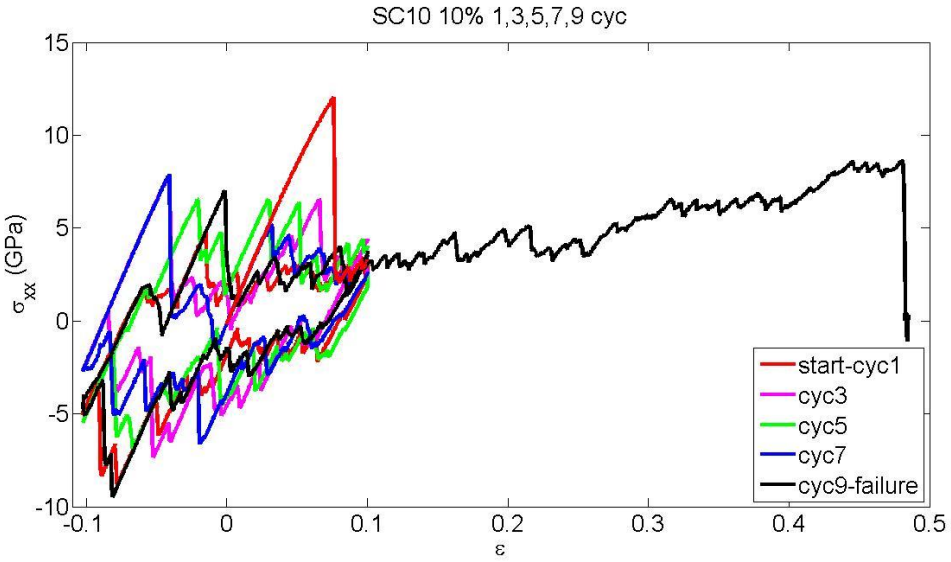

Fig. 3.1 σ-ε curves for Cu single crystal during nine tension-compression cycles in the strain range of $\pm 10\%$.

3.2 Observations and Discussion

3.2.1 Bauschinger effect

To obtain a general view of Bauschinger's effect in copper, three identical

Cu systems were deformed with cyclic tension-compression processes in different strain ranges, ±10%, ±15%, and ±20%, along X axis. Fig.3.2. illustrates first deformation cycle for the three different strain ranges. The samples were initially pulled to reach maximal strains of 10%, 15% and 20%, respectively. Then cyclic loading was started with compression. As shown, after the system was compressively deformed, the resistance to plastic deformation during the following tension process became quite lower, less than 2GPa (see Fig.3(a)), compared to that in the yielding point in the first cycle(about 12GPa) as shown in Fig.3.1, confirming the Bauschinger's effect.

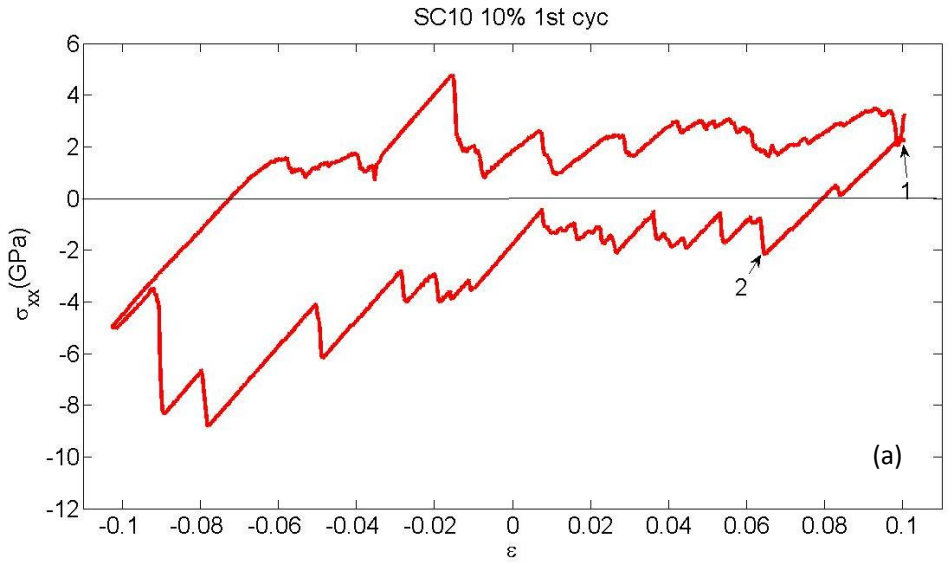

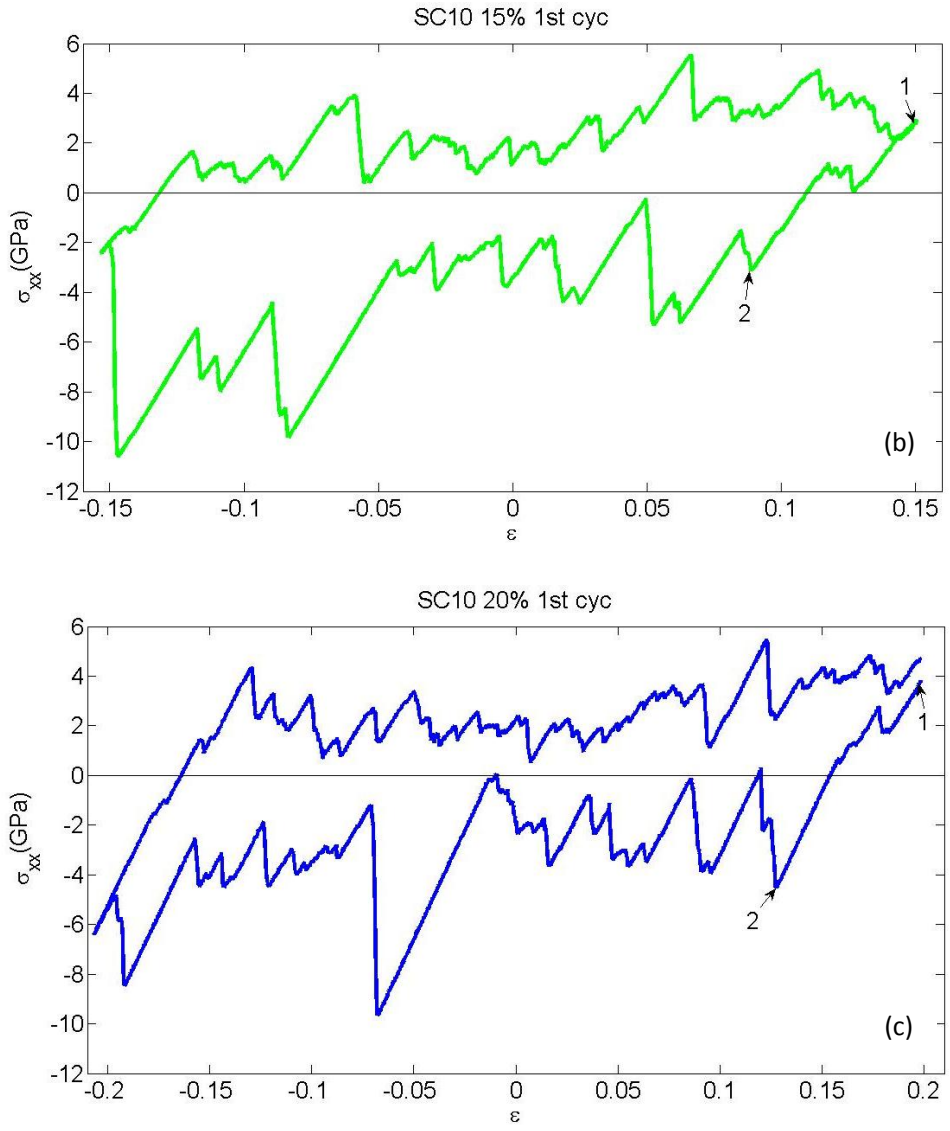

Fig.3.2 σ-ε curve in the first cycle for single crystal with tension-compression range of ε respectively equal to (a)± 10%, (b)± 15%, (c)± 20%. The starting point is marked with "1".

During the loading process, the magnitude of stress gradually increased owing to the strain-hardening effect. Two phenomena were noticed: 1) strain-hardening was more obvious during the compression process; 2)

Bausinger's effect was more obvious when the stress is reversed from compression to tension. These could result from a change in the barrier to the dislocation movement or generation under different stress conditions. In general, the movement of dislocations or partial dislocations occurs under a shear stress as Fig.3.3 illustrates.

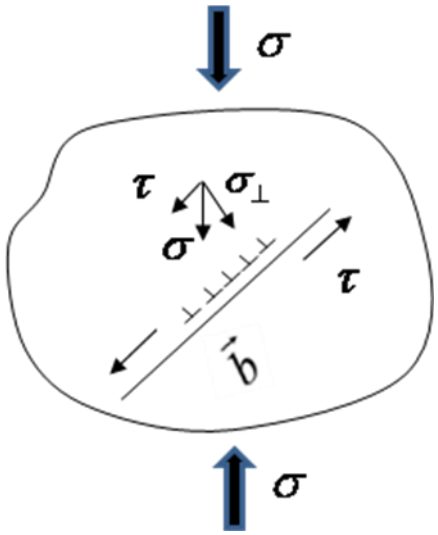

Fig.3.3 Slip is more difficult under compression than under tension due to the variation in the atomic spacing on the slip plane, which affects Burger's vector.

Under compression, the operation of slip systems may become more difficult. As shown in Fig.3.3, under a global compressive stress (σ), the local compressive compound $\sigma_{\perp}$ normal to the slip plane expands the lattice along the direction perpendicular to $\sigma_{\perp}$. This lattice expansion increases the magnitude of Burgers vector ($\vec{b}$) and thus the difficulty for dislocations to nucleate and glide on the slip plane. The increase in the magnitude of Burgers

vector may be estimated as [16]

$$\left|\Delta\vec{b}\right| = \left|-\nu\frac{\sigma_{\perp}}{E}\vec{b}\right| = \nu\frac{\left|\sigma_{\perp}\right|}{E}b \qquad (1)$$

where E and ν are the elastic modulus and poisson ratio of the material. The frictional stress (τ_f) for dislocation movement is affected by lattice parameters [65], which is given by

$$\tau_f = \frac{2G}{1-\nu}\exp[\frac{-2\pi a}{(1-\nu)b}] \qquad (2)$$

where G is the shear modulus and a is the lattice spacing perpendicular to $\vec{b}$. When the lattice is distorted, the frictional stress changes and such change may be represented as

$$\Delta\tau_f = \frac{2G}{1-\nu}\exp(-\frac{2\pi a}{(1-\nu)b})[-\frac{2\pi}{(1-\nu)b}\Delta a + \frac{2\pi a}{(1-\nu)b^2}\Delta b] \qquad (3)$$

Approximately, we may assume that $a \sim b$ and taking account of the following relationships of $\Delta b = -\nu\frac{\sigma_{\perp}}{E}b$ and $\Delta a = \frac{\sigma_{\perp}}{E}a$, $\Delta\tau_f$ may thus be estimated as

$$\Delta\tau_f \cong \tau_f\frac{-2\pi\sigma_{\perp}}{(1-\nu)E}(1+\nu) \qquad (4)$$

Equation (4) indicates that compressive stress increases the frictional stress for dislocation movement, thus resulting in a larger resistance to plastic deformation when the same type of defects pile up, leading to an enhanced strain-hardening effect, compared to that occurring in a tension process. Such

a mechanism is also applicable to the second phenomenon. When piled up dislocations in front of an obstacle caused by tension start to move backwards as the stress is reversed, the change in the magnitude of Burgers vector is actually doubled (i.e. $2\left|\Delta\vec{b}\right|$, caused by the stress reversal). This increases the barrier to the backward movement of the dislocations. As a result, the "softening" effect occurring during the stress reversal from tension to compression is weaker than that occurs during the stress reversal from compression to tension. Or in other words, Bauschinger's effect is asymmetrical with respect to the stress type. This asymmetry may also be seen from changes in the defect amount during a tension-compression cycle. Fig.3.4 illustrates representative changes in the number of atoms associated with defects during 7^{th} and 8^{th} tension-compression cycles. As shown, overall the number of defect-atoms during compression is smaller than that during tension, which may correspond to the larger barrier to the generation of defects during compression process. In order to accommodate deformation, larger stress is needed.

It should be mentioned that the number of defect-atoms has large fluctuations, reflecting the generation and cancellation or vanishing of defects during the loading processes.

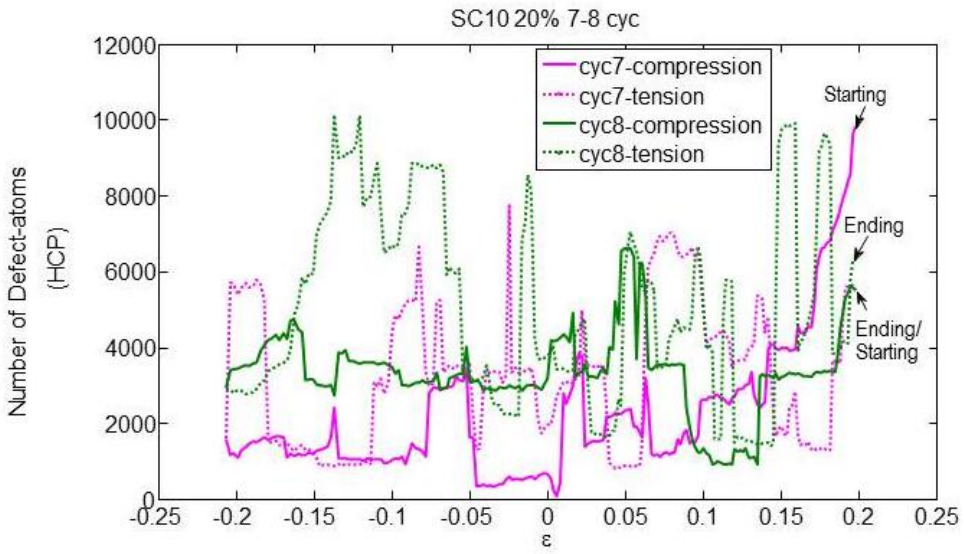

Fig.3.4 Variations in the number of atoms associated with defects during 7th and 8th tension-compression cycles; strain range = ± 20%.

Regardless of the above-discussed asymmetrical Bauschinger's effect, the reduction of defect number associated with Bauschinger's effect generally occurred with the stress reversal. Fig.3.5 illustrates configurations of the system when the stress was changed from tension (point 1) to compression (point 2) as marked in Fig.3.2. The decrease in the defect number as the stress reversal is an indication of Bauschinger's effect.

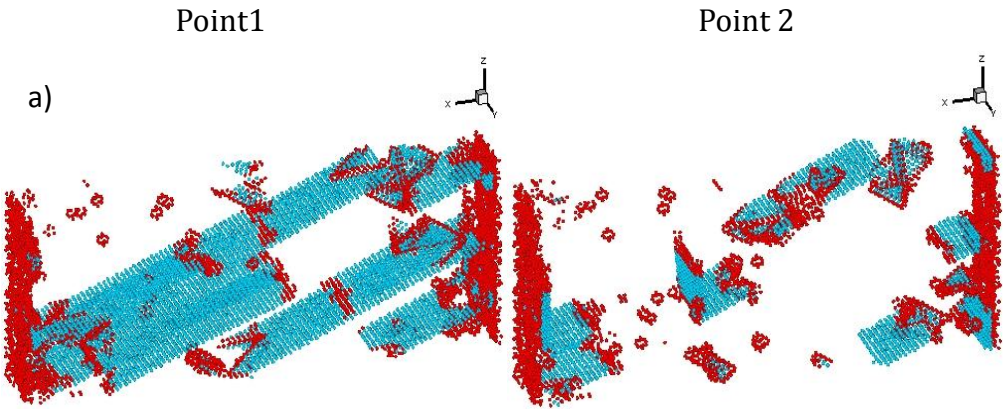

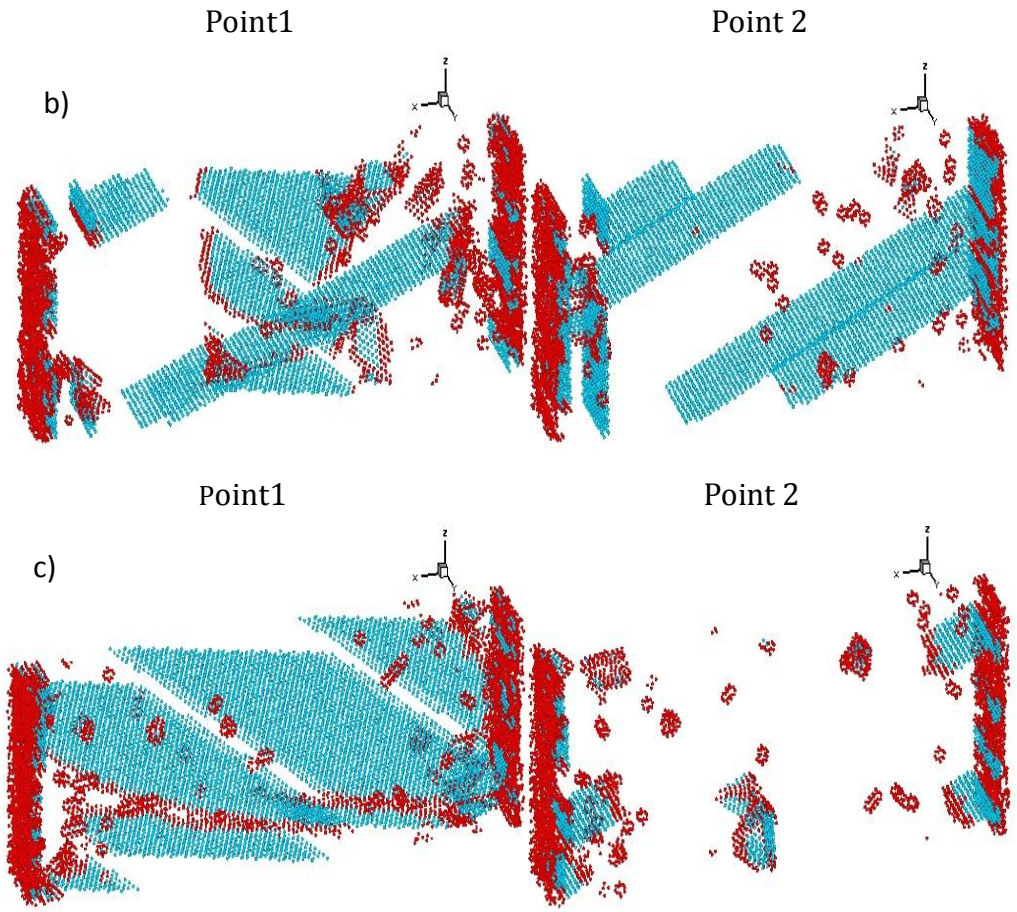

Fig.3.5 Configurations of the system when the stress was changed from tension (point 1) to compression (point 2) as marked on the stress-strain curves shown in Fig.3.2. Form point 1 to point 2, atoms in stacking faults (in blue) and those belong to partial dislocations and other defects (marked in red) decrease. (a) strain range = ± 10%, (b) strain range = ± 15%, and (c) strain range = ± 20%.

Point 2 is the point where massive plastic flow starts under compression. The stress at this point changes with the maximum strain magnitude. In the present case, $|\sigma_{xx}|$ at point 2 increases from 2.098GPa through 2.984GPa to 4.44GPa as $\varepsilon_{\max}$ increases from 10% through 15% to 20%. This increase in the stress magnitude corresponding to the occurrence of massive plastic flow

is a result of raised barriers to the reversible movement of partial dislocations and associated shrinkage of stacking faults, which could result from enhanced defect interactions when the total defect amount is elevated with an increase in the strain range. With an increase in deformation, the “free” space for defect to move is reduced and Bauschinger’s effect may become more localized.

3.2.2 Fluctuation on σ-ε curve

The σ-ε curve is not smooth with fluctuations as illustrated in Fig.3.2, which is common for systems experienced deformation in different strain ranges. The fluctuations could be attributed to the existence of local barriers for dislocations to move along with the extension of associated stacking faults. Fig. 3.6 illustrates changes in configuration corresponding to the fluctuations as marked on the stress-strain curve shown in the figure. As illustrated, from points 1–3, the configuration does not change much, implying that the system defects are pinned or blocked. Only when the local stress is larger enough to break the blocking, defect movement or extension occurs as shown in Fig.3.6.

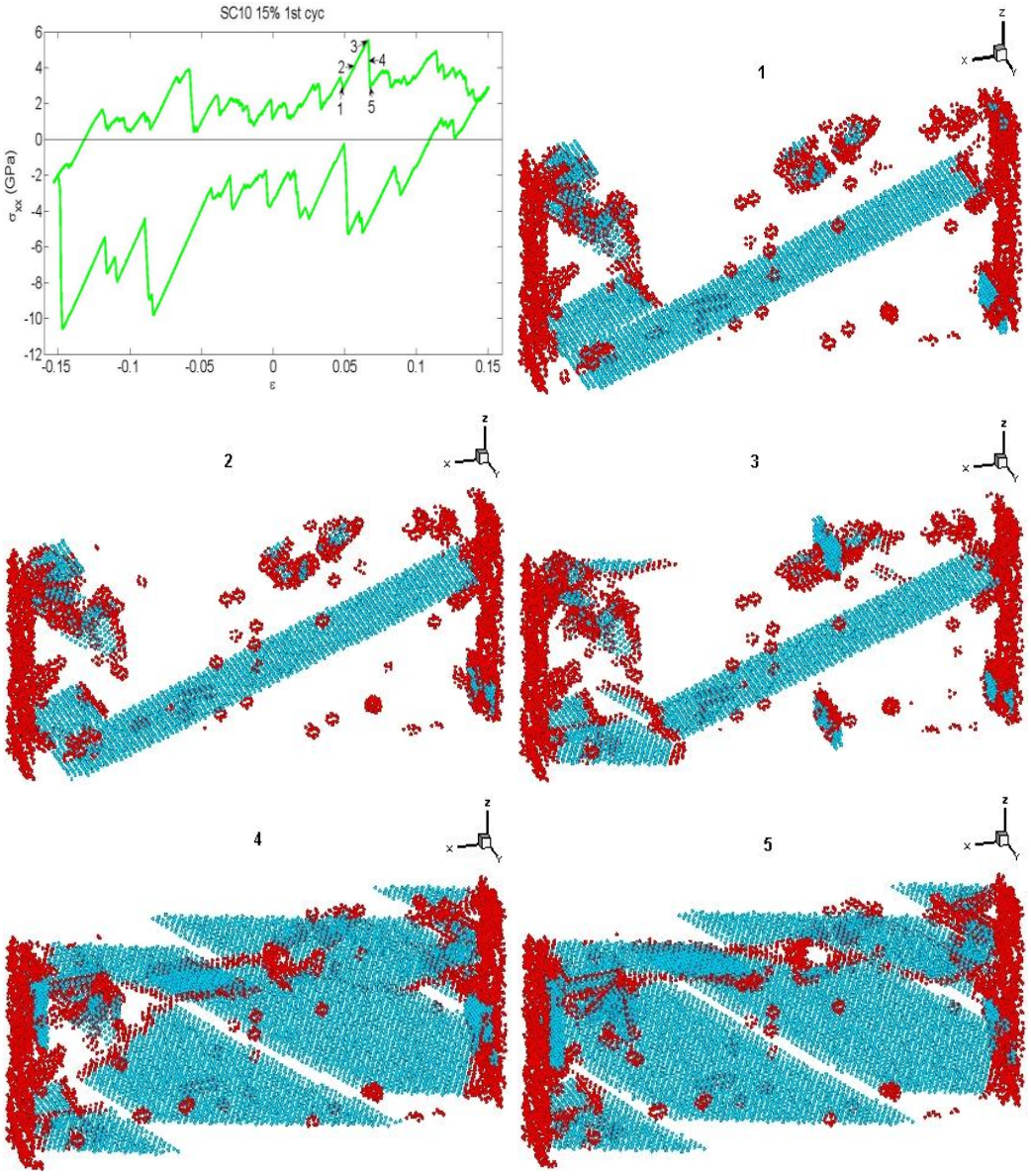

Fig.3.6 Changes in configuration corresponding to the fluctuations as marked on the σ-ε curve during the first cycle in the strain range of ± 15%; Corresponding configurations of 5 marked points are presented.

The fluctuation of σ-ε curve appears independent on the number of compression-tension cycles and the strain range as shown in Fig.3.7, which illustrates σ-ε curves of 1st, 5th and 9th cycles for three different strain ranges.

The independence of the fluctuation on the number of cycles and the strain range may imply that Bauschinger's effect involving reversible movement and annihilation of defects could play a role in keeping the material in a relatively stable state without continuously build up defect quantities and stress concentrations.

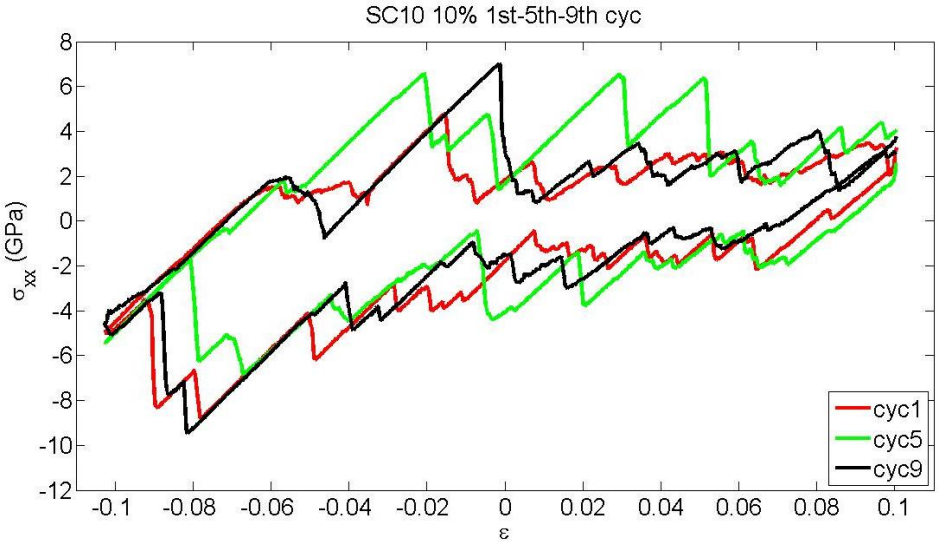

(a)

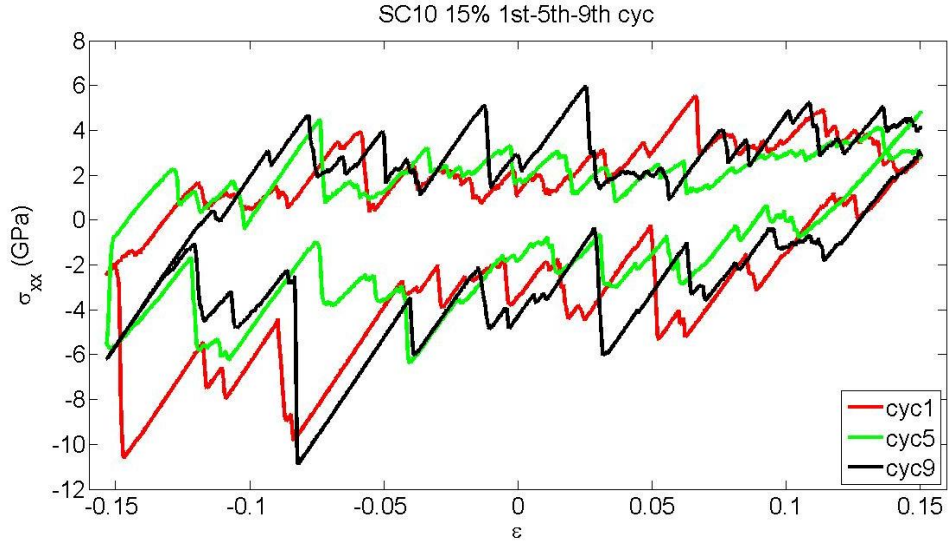

(b)

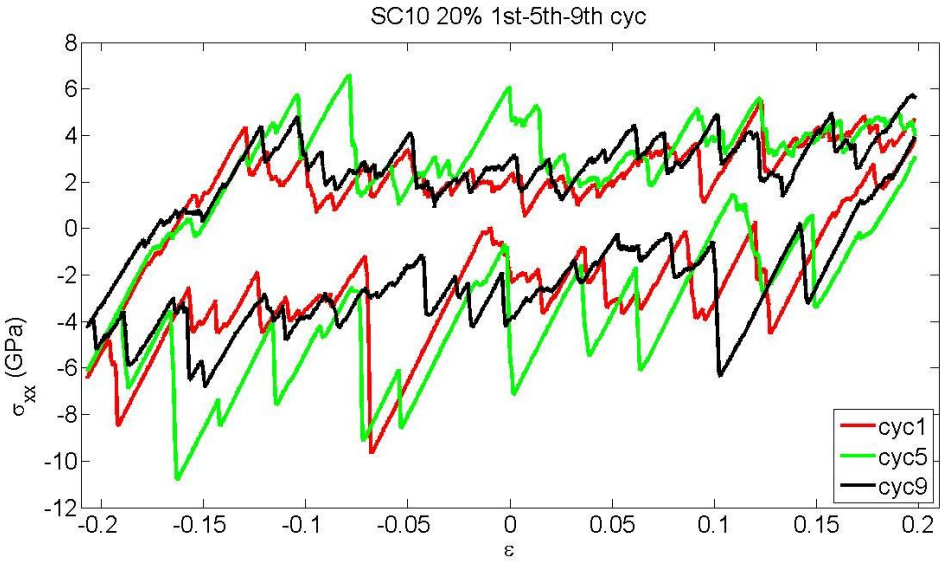

(c)

Fig.3.7 σ-ε curves of 1st, 5th and 9th cycles for three different strain ranges: (a) Strain range = ± 10%, (b) strain range = ± 15%, and (c) strain range = ± 20%.

3.2.3 Increase in the failure strain with the cyclic loading

During the simulation, unexpectedly, it was interesting to observe that the fracture strain increased with the number of stress cycles. Failure strains at the end of different stress cycles were determined. The failure strain is defined as the ratio of the elongation over the total length of a system. The elongation is the difference between the final length at failure and the stress-free length of the system regardless of its deformation history. The failure strain is calculated as follows:

Original length: L_0

Length with residual strain after cycling: $L_0' = L_0(1+X_1)$

Failure length: $L = L_0(1+X_2)$;

Deformation quantity: $\Delta L = L - L_0' = L_0(1+X_2) - L_0(1+X_1) = L_0(X_2-X_1)$;

Percent elongation(Engineering): $\%EL_{engineering} = \Delta L / L_0' = L_0(X_2-X_1) / (L_0(1+X_1)) = (X_2-X_1)/(1+X_1)$.

Percent elongation(True): $\%EL_{true} = Ln(1 + \%EL_{engineering})$

where X_1 and X_2 represent strains at points shown in Fig.3.8(a).

Based on results of the simulation, the failure strains of systems experienced single-pulling and nine stress cycles at strain=10%, 15% and 20%, are given in Table 3.1. Corresponding up-to-failure σ-ε curves are illustrated in Fig.3.8 (b).

Table 3.1 - Failure strains of systems experienced single-pulling and nine stress cycles at strain=10%, 15% and 20%, respectively

ε	X_1	X_2	$\%EL_{engineering}$	$\%EL_{true}$
0% (tensile test)	0	0.4279	42.79%	35.62%
± 10%	-0.07182	0.4803	59.48%	46.68%
± 15%	-0.1174	0.5396	74.44%	55.64%
± 20%	-0.1738	0.544	86.88%	62.53%

(a)

(b)

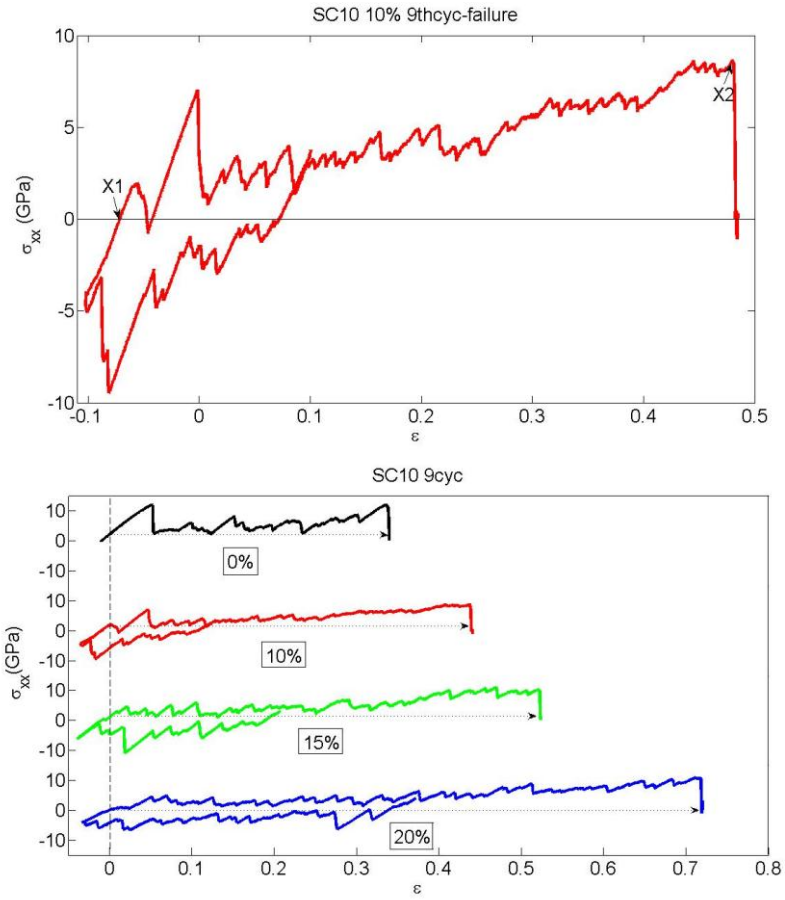

Fig.3.8 (a) A representative σ-ε curve of a model system up to failure after ninth cycle (strain range: ±10%), on which X_1 and X_2 are marked; (b) up-to-failure σ-ε curves of samples after experiencing nine cycles in different strain ranges: 0%, ±10%, ±15%, ±20%, respectively.

As shown in Table 3.1 and Fig.3.8(b), the bidirectional loading may lead to larger failure strain, and increasing the cyclic strain range raises the fracture strain. These could be explained as follows. For single pulling, similar type defects are generated and piled up by obstacles (mainly defect interactions in a single crystal system), leading to higher stress concentrations. As a result, the

material may have a higher failure probability and fails when the concentrated stress reaches a critical value. For bidirectional loading, the reversible dislocation movement, cancellation of the defects with opposite signs, and shrink of stacking faults may diminish the build-up of local stress or stress concentrations. When subsequently pulled to failure, the resultant deformation is accommodated not only by generation of new defects but also cancellation of dislocations with opposite signs as well as changes in defect arrangement. As a result, the material could show an increased strain prior to failure after experiencing compression-tensile cyclic loading. Increasing the strain range may help defects to overcome barriers to their reversible movement and rearrangement due to the Bauschinger "softening" effect, thus further raising the fracture strain.

It should be indicated that the above phenomena demonstrated by the simulation of a single crystal system may not be revealed during macroscopic deformation of polycrystalline materials subjected to cyclic loading, in which the grain boundaries and complex deformation process may largely alternate the situation. This will be discussed in details in Chapter 5.

3.2.4 Energy absorbed in the cyclic loading process

A deformed system has elevated internal energy, which continuously

increases by further deformation up to failure. The absorbed energy of the system was calculated using the equation: $U = \int_{-|\varepsilon_{tc}|}^{+|\varepsilon_{tc}|} (\sigma_{xx\_tension} - \sigma_{xx\_compression}) d\varepsilon$, for each tension-compression cycle. Here $|\varepsilon_{tc}|$ equaled to 10%, 15%, or 20%. As shown in Fig.3.9, the energy increases with the strain range ($|\varepsilon_{tc}|$) and the energy fluctuates with the number of cycles. As shown, the energy is basically stable within a certain energy range, indicating that the plastic compression-tension cycles do not continuously increase the internal energy or average defect quantities although fluctuations exist as shown in Fig.3.10. Bauschinger's effect should play a role in keep the overall energy stable. The energy fluctuation with respect to the loading cycles is an indication that the energy is self-adjusted during the tension-compression loading cycles.

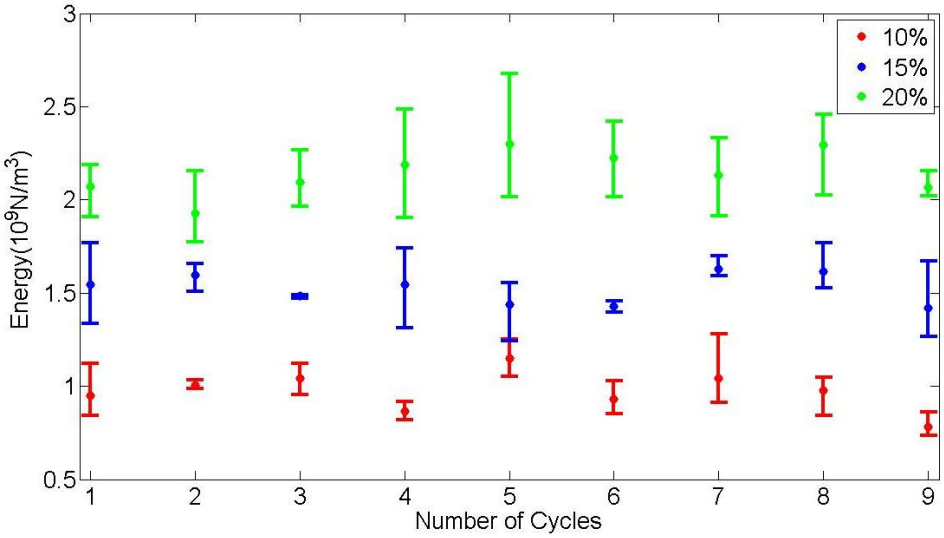

Fig.3.9 The energy absorbed during the tension-compression loading cycles with the strain ranges equal to ± 10%, ± 15%, and ± 20%, respectively.

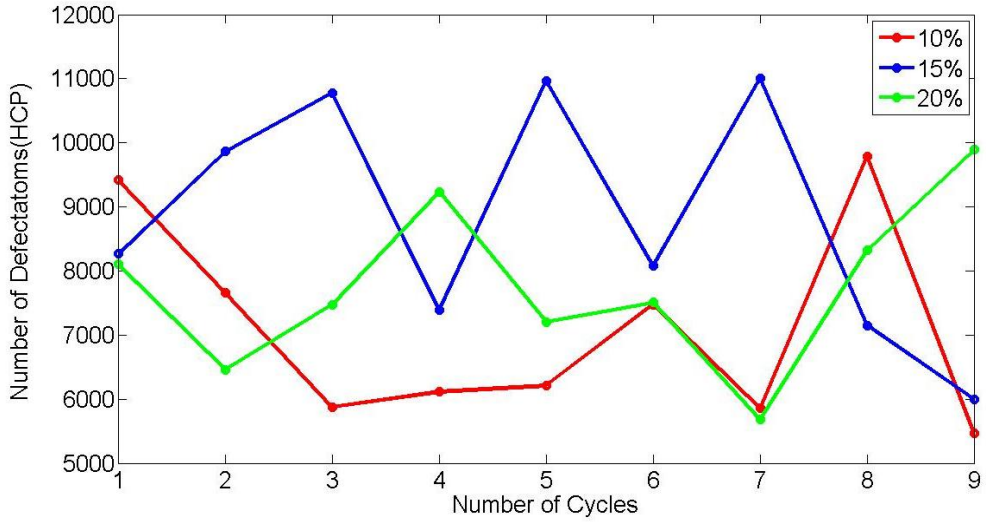

Fig.3.10 The average numbers of defect-atoms for different cycles with the strain ranges equal to ±10%, ±15%, and ±20%, respectively.

3.3 Summary

A molecular dynamics simulation study was conducted to investigate the response of copper single crystal to cyclic loading in the strain ranges of ±10%, ±15%, and ±20%, respectively. Bauschinger's effect occurring during the cyclic loading process was demonstrated and relevant phenomena were analyzed. The following conclusions are drawn:

1) Bauschinger's effect is asymmetrical with respect to the stress type. Softening is more obvious when the stress is reversed from compression to tension. Strain- hardening is stronger under compression than under tension.

2) The independence of the fluctuation on σ-ε curve on the number of cycles and the strain range may imply that Bauschinger's effect involving reversible

movement and annihilation of defects could play a role in keeping the material in a relatively stable state without continuously increasing the defect quantities and stress concentrations.

3) The fracture strain is increased by tension-compression cyclic loading, which may result from the Bauschinger's "softening" effect due to reversible movement of defects and cancellation of dislocations with opposite signs.

4) The energy is self-adjusted during the tension-compression cycles; the energy is relatively stable within a certain energy range, indicating that the bidirectional cyclic loading does not continuously increase the average internal energy or defect quantities although fluctuations exist, which is ascribed to the Bauschinger's effect.

Chapter 4 Influence of nano-twin boundary on the Bauschinger's effect in Cu

In this chapter, effects of twin boundary (TW) as an ordered obstacle in nano-scaled Cu crystal on defects' generation and annihilation during cyclic tension-compression loading processes were investigated, in comparison with those occurring in a single crystal (SC). For self-containing comparison purpose and some relevant results for SC are represented in this chapter. It was observed that the Bauschinger's effect in the nano-scaled TW system was weaker with higher residual strain energy, compared to the SC system; and the ductility of both the SC and TW systems was increased by the cycling loading but this increase was smaller for the TW system. Efforts are made to elucidate mechanisms involved.

4.1 Bauschinger effect in nanocopper with twin boundaries

To investigate the effect of twin boundaries on Bauschinger's effect, Both the TW and SC samples were deformed with cyclic tension-compression processes, with a loading rate equal to $10^7 s^{-1}$, in three strain ranges, $\pm 10\%$, $\pm 15\%$ and $\pm 20\%$, along x axis. Fig.4.1 illustrates tension-compression cyclic $\sigma - \varepsilon$ curves of TW and SC systems within the strain range of $\pm 10\%$, $\pm 15\%$

and $\pm 20\%$.

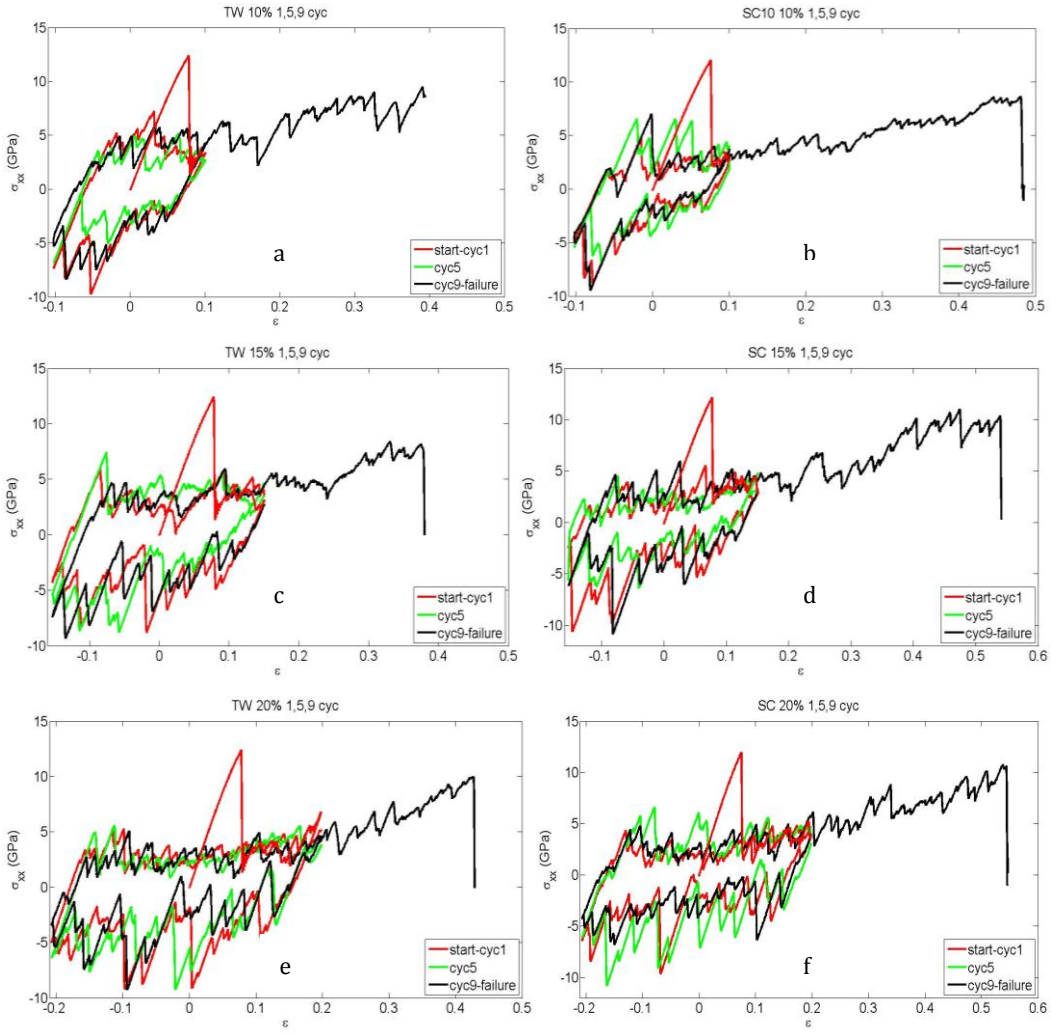

Fig.4.1 Tension-compression cyclic σ-ε curves under different loading conditions with cyclic strain range was equal to (a) ± 10% in the TW system; (b) ± 10% in the SC system; (c) ± 15% in the TW system; (d) ± 15% in the SC system; (e) ± 20% in the TW system; and (f) ± 20% in the SC system.

As shown, during initial pulling, plastic deformation occurred in the TW system at a yield stress of about 12.35 GPa, while the material initally yielded at a stress around 11.96GPa in the SC system. The higher yield stress of the TW system resulted from the twin boundaries which raised the barrier to

plastic deformation. After nine cycles, the systems were pulled up to failure. The TW system fractured at a stress of 9 GPa while the SC system fractured at a lower stress around 7.5 GPa when the systems were cyclically loaded within the strain range of 10%. However, for cyclic loading in the strain ranges of 15% and 20%, the fracture stresses after nine cycles were 10.4GPa and 10.74GPa for the SC system, and 8.158GPa and 10GPa for the TW one, respectively. Theoretically, the TW system should have a higher ultimate strength and fail at a higher stress; however the observed relatively lower failure stresses of the TW system in the larger strain ranges (15%, 20%), compared to those of the SC system, may imply that stress concentrations could be built up faster in the TW system, leading to its lower fracture stress in contrast with that of the SC system when the cyclic strain range was increased.

It should be mentioned that the above processes occurred on the nano-scale, so it is more appropriate to use the flow stress to represent the stress corresponding to the occurrence of plastic deformation. However, for simplicity we call the critical point at which plastic deformation occurs as the yielding point. In order to make adopted terminologies consistent, the yield stress rather than flow stress is still used for the nano-scale systems.

For a closer look, first cycles of the TW and SC systems in strain ranges of

10%, 15% and 20% are illustrated in Fig.4.2. The systems were initially pulled to maximal strains of 10%, 15% and 20%, respectively. Then cyclic loading was started with compression. As shown, after the system were

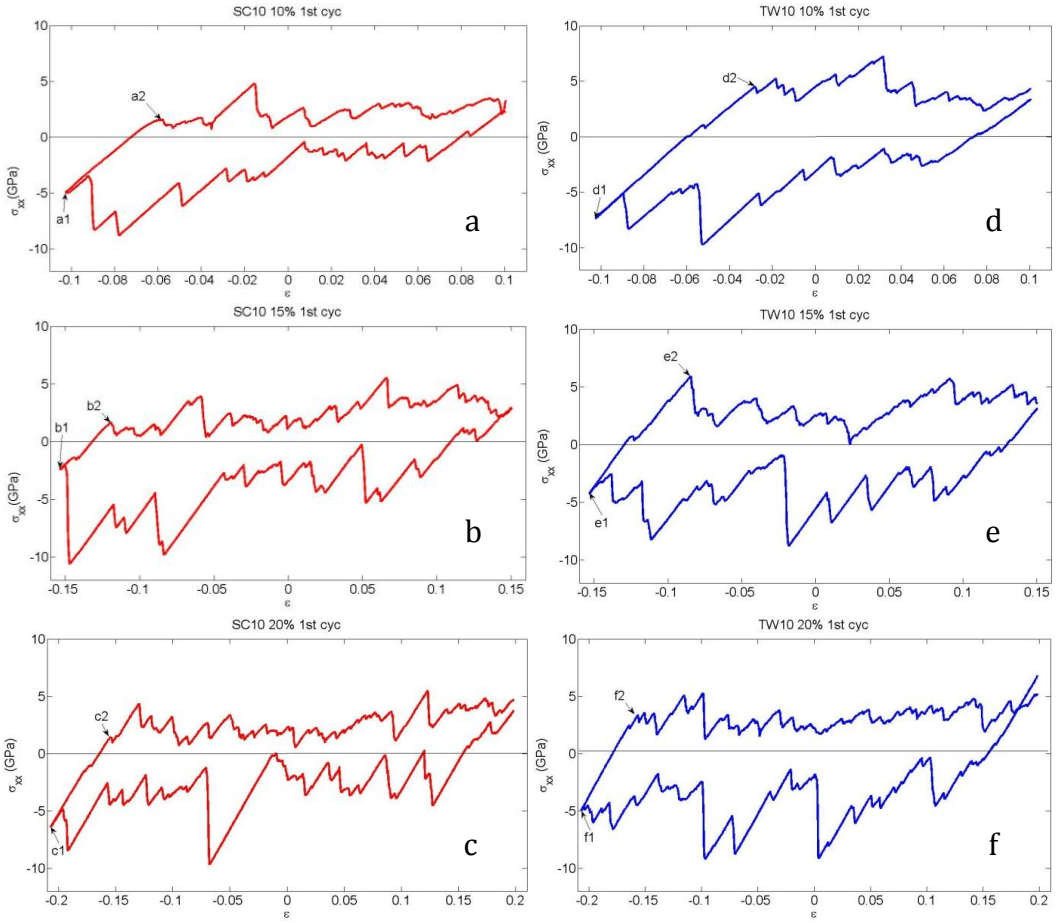

Fig.4.2 σ-ε curves in the first cycle respectively for SC and TW system with three different tension-compression ranges of ε: (a) SC with a strain range equal to ± 10%, (b) SC with a strain range equal to ± 15%,(c) SC with a strain range equal to ± 20%, (d) TW with a strain range equal to ± 10%, (e) TW with a strain range equal to ± 15%, (f) TW with a strain range equal to ± 20%. Ends of compression processes are marked with "a1","b1","c1","d1","e1" and "f1", respectively, while the yielding points after compressive deformation are marked with "a2","b2","c2","d2","e2" and "f2", respectively .

compressively deformed, their resistance to plastic deformation during the

following tension process became lower, about 5GPa for TW (see d2, e2 and f2 respectively in Fig.4.2(d), Fig.4.2(e) and Fig.4.2(f)), compared to that at the yielding point when the system was pulled during the first tensile process (about 12.5GPa) as shown in Fig.4.1, demonstrating the Bauschinger's effect in the TW system with two nano-twin boundaries.

The situation of the SC system is similar but the tensile yield stress decreased to a value smaller than 2GPa (see a2, b2 and c2 respectively in Fig.4.2(a), Fig.4.2(b) and Fig.4.2(c)), indicating that Bauschinger's effect was less profound in the TW system. In order to statistically evaluate the effect of nano-twin boundaries on Bauschinger's effect, a parameter called B-asymmetry is defined, which is the absolute ratio of the maximum stress before the stress reversal to the yielding stress of the subsequent reversed loading process, to reflect the degree or strength of the Bauschinger's effect. The larger the value of B-asymmetry, the stronger the Bauschinger's effect. If there is no Bauschinger's effect, this value is one. B-asymmetries of all cycles were averaged for the TW and SC systems (in all strain ranges including 10%, 15% and 20%), respectively, and are presented in Fig.4.3. As shown, overall, the nano-twinned copper shows a lower degree of Bauschinger's effect.

Fig.4.3 Average values of B-asymmetry of the TW and SC systems. The data were obtained by averaging the ratios of the maximum compressive stress to the yielding stress of the subsequent tension process of all loading cycles applied to the TW and SC systems, respectively.

The lower degree of Bauschinger's effect of the nano-twinned system is different from expectation, which could result from the constraint of the small spacing between the two twin boundaries on dislocation movement. In nanocrystalline copper, plastic deformation is largely achieved by generating stacking faults, which extend through the movement of partial dislocations at the edge of the stacking faults [26]. When the spacing between two twin boundaries is reduced to nanometer scale such as 10 nanometers in the present case, the free space is limited for the partial dislocation to move backwards as the applied stress is reversed. In addition, unlike a grain boundary which may act as a sink for dislocations, the twin boundary hardly accommodates dislocations. These could negatively affect the reversible

movement of partial dislocations and associated stacking faults. As a result, Bauschinger's effect could be weakened. The atomic configurations at yielding points (a2, b2, c2, d2, e2 and f2) in the first cycle after compressive deformation as well as at the end points of the compression process (a1, b1, c1, d1, e1 and f1) as marked on the σ-ε curves of the systems in Fig.4.2 are examined and presented in Fig.4.4. As shown, the twin boundaries with nano-scaled spacing may not favor the defect reversible movement. In the SC system, partial dislocations move backwards with associated stacking faults extended to the edge of the SC system when yielding occurred during pulling after the compression process. While in the TW system, fewer stacking faults were generated during the pulling process and stack fault extension is limited or blocked by the twin boundary as illustrated, e.g., in Fig.4.4 f2.

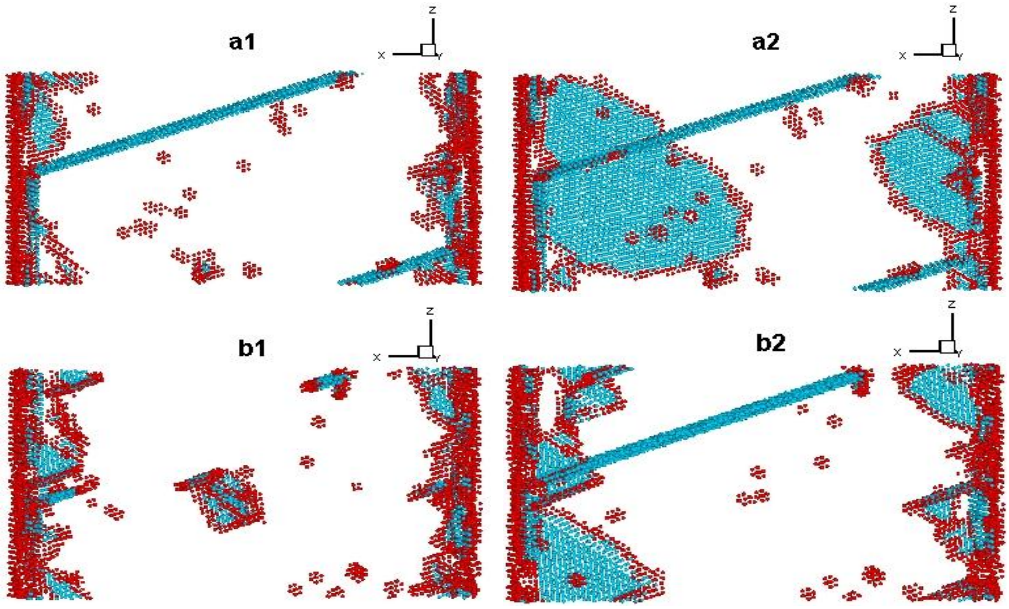

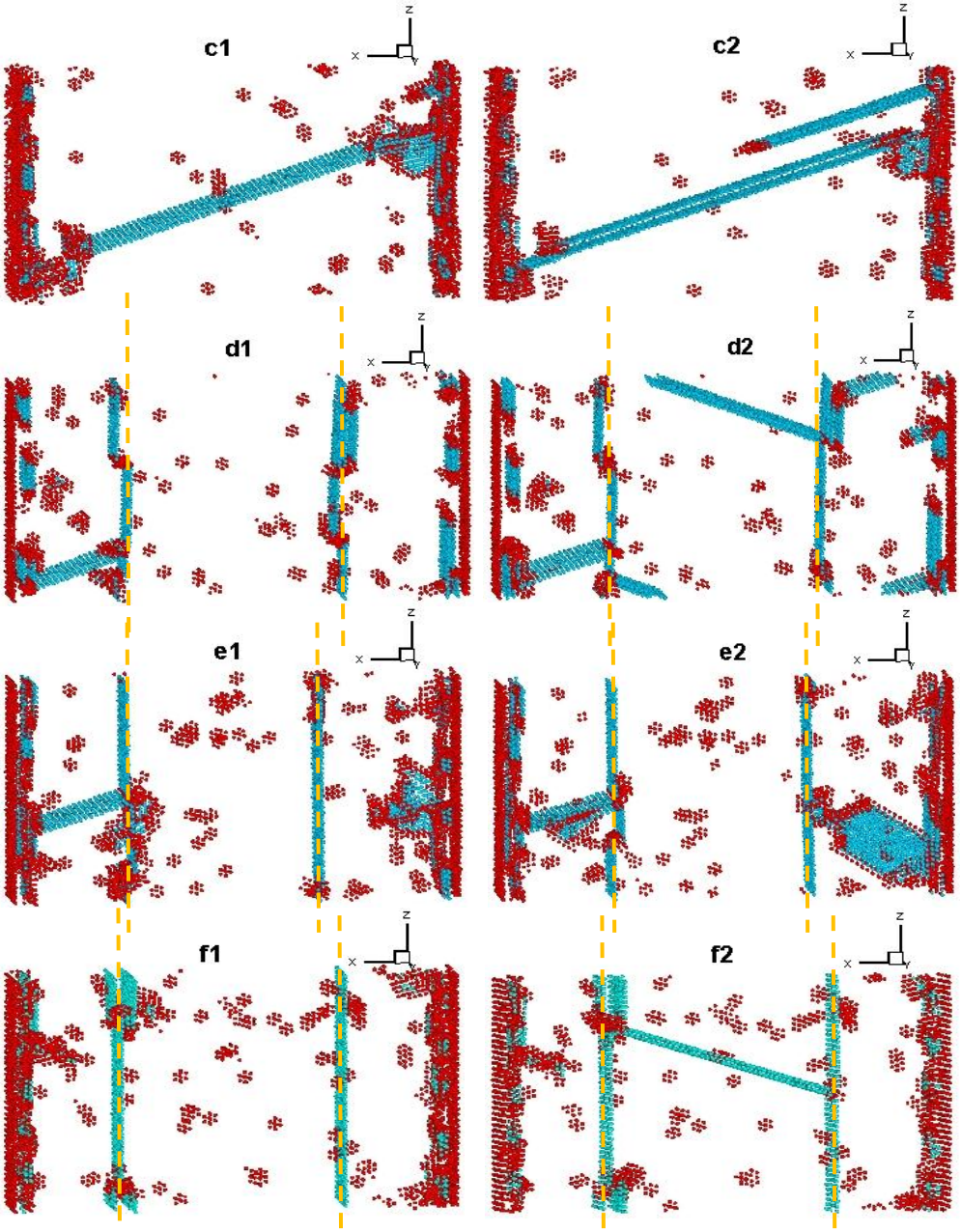

Fig.4.4 Configurations corresponding to the yielding points in the first cycle after compressive deformation as marked as a2, b2, c2, d2, e2 and f2 on the σ-ε curves in Fig.4.2. Configurations at the end of prior-compression process are also presents, corresponding to points as marked as a1, b1, c1, d1, e1 and f1 on σ-ε curves in Fig.4.2. Blue areas are stacking faults and TW boundaries, and the red areas represent other defects, e.g., clusters of vacancies. (Initial twin boundaries are marked with dash lines.)

Besides, one may see that there were more clusters of other types of defects (marked in red in Fig.4.4) generated in the TW system during the compression process before pulling. It appears that these defect clusters along with the TW boundaries helped suppress or block the extension of stacking faults. These obstacles are responsible for the higher yield strength of the TW system for the second loading cycle, compared to the situation of SC system. The formation of more defect clusters might be ascribed to the interference of the twin boundaries to the homogeneity or continuity of the applied stress and complicated strain process [66-68].

The higher reversibility of defects in the SC system, compared to that of defects in the TW system on the nano-scale, may also be seen from local events related to defect activities when the applied stress was released. Fig.4.5 and Fig.4.6 illustrate $\sigma-\varepsilon$ curves and a few corresponding configurations. As shown, when the SC system was unloaded from a tension state (a1–a2 in Fig.4.5(a)), a large amount of stacking faults vanished (Fig.4.6), while in the TW system, the change in defect state was much smaller as the tension was released to zero. Such a difference in defect activity between the SC and TW systems during unloading suggests that defects in the TW system at the nano-scale were not as reversible as those in the SC system.

(a)

(b)

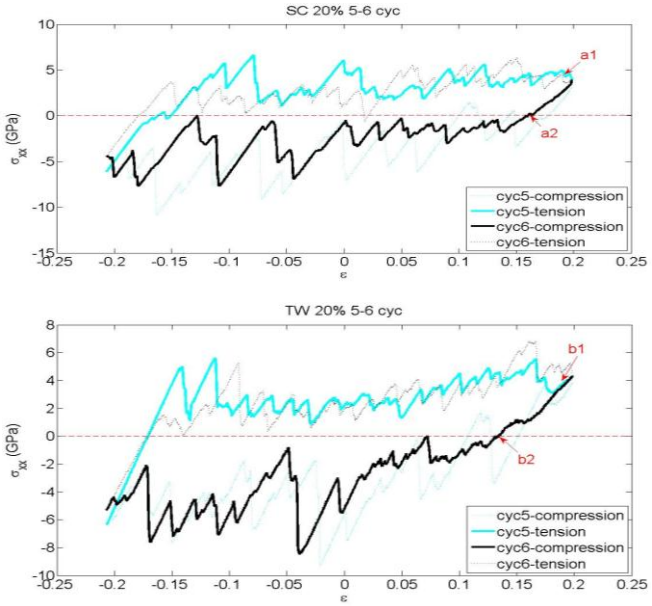

Fig.4.5 σ-ε curves in the 5th and 6th cycle of (a) a SC system; (b) a TW system. The cyclic strain range was ± 20%.

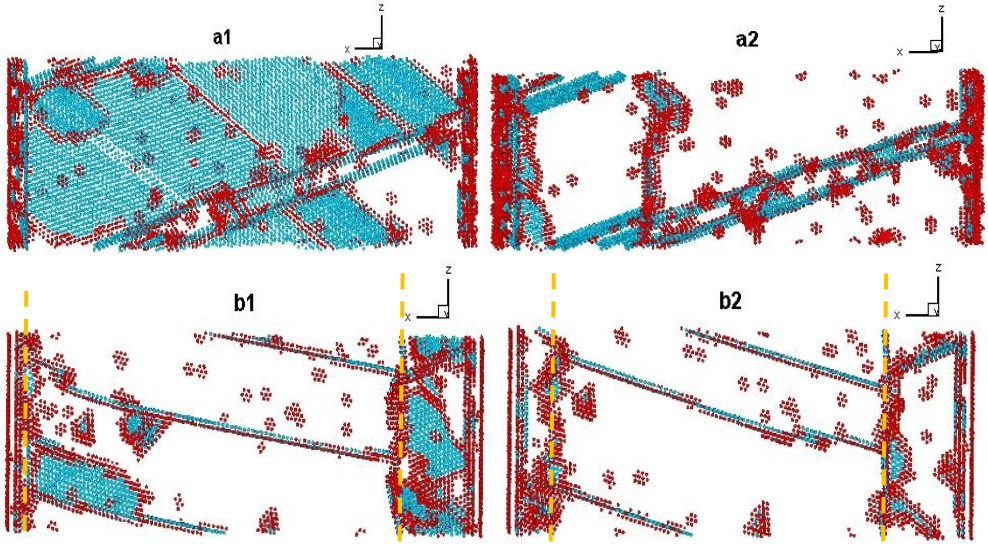

Fig.4.6 Configurations corresponding to the maximum tensile stress, marked as a1 for the SC system and b1 for the TW system during the 5th cycle in Fig.4.5; and configurations corresponding to zero-stress states marked as a2 and b2, respectively. Blue areas represent stacking faults and TW boundaries, while red areas represent other defects, e.g., clusters of vacancies. (Initial twin boundaries are marked with dash lines.)

In summary, unlike the case of coarse grained crystals with twin boundaries in which dislocations accumulated in the front of twin boundaries could be easier to be pushed away when stress is reversed, in the nano-twinned crystal, the small spacing between ordered twin boundaries may largely limit the defect movement and stacking fault extension or shrinkage (i.e. less reversible), and thus weakens the Bauschinger's effect. The TW boundaries also facilitate the formation of defect clusters, generating additional barriers to the stacking faults.

4.2 The failure strain with the cyclic loading

The previous chapter has shown that the tension-compression cyclic loading may change the failure strain of Cu single crystal. It is of interest to see how the TW boundaries affect the failure strain after experiencing tension-compression cyclic loading. The definition of failure strain is defined in chapter 3, i.e. the difference between the final length at failure and the stress-free length of the system regardless of its deformation history:

Percent elongation (Eng.): $\%EL_{engineering}=(X_2-X_1)/(1+X_1)$

Percent elongation (True): $\%EL_{true}=Ln(1+\%EL_{engineering})$

where X_1 and X_2represent strains at points shown in Fig.4.7.

Up-to-failure σ-ε curves of TW samples after experiencing nine cycles in different strain ranges: 0%, ±10%, ±15% and ±20%, respectively, were obtained from the simulation. Values of the failure strain of the TW systems are given in Table 4.1. Corresponding up-to-failure σ-ε curves are illustrated in Fig.4.8, in which the failure points after deformation are marked with "a", "b", "c", "d", "e", "f", "g", and "h", in comparison with that in the SC system.

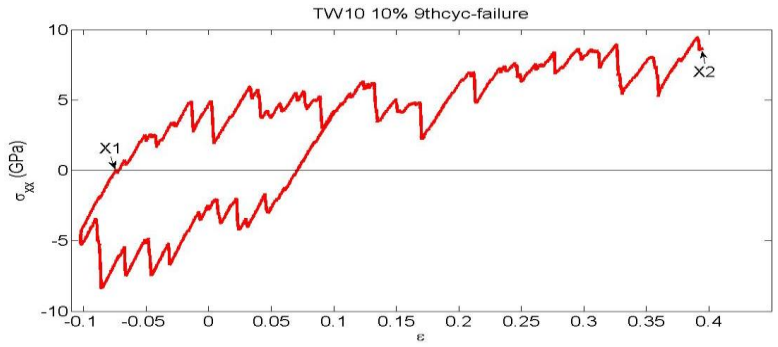

Fig.4.7 A representative σ-ε curve of a model system up to failure after ninth cycle, in which X_1 and X_2 are marked.

Table 4.1 - Failure strains of the TW system experienced single-pulling and nine stress cycles at strain=10%, 15% and 20% , respectively

System	ε	X_1	X_2	$\%EL_{engineering}$	$\%EL_{true}$
Twin Boundary	singlepulling	0	0.3648	36.48%	31.10%
	±10%	-0.07143	0.3945	50.18%	40.67%
	±15%	-0.1089	0.3787	54.72%	43.65%
	±20%	-0.1709	0.4272	72.14%	54.31%

As illustrated in Fig.4.8, the cyclic loading increased the ductility of failure

strain of the TW and the increment was higher as the strain range was increased. The increase in ductility by the tension-compression cyclic loading could be attributed to the reversible defect movement or stacking fault shrinkage as well as possible cancellation of dislocations with opposite signs as the stress is reversed, thus reducing the stress build-up or lowering the stress concentration. As a result of the favorable change in local stress, the failure strain is increased.

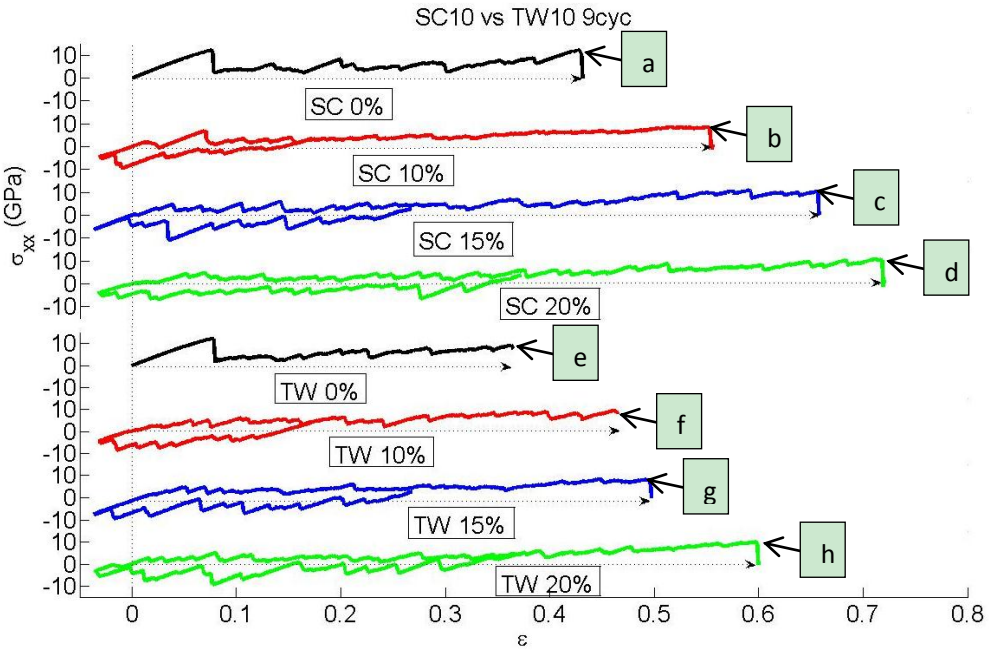

Fig.4.8 Up-to-failure σ-ε curves of SC and TW samples after experiencing nine cycles in different strain ranges: 0%, ±10%, ±15% and ±20%, respectively. The failure points after deformation are marked with "a","b","c", "d", "e", "f", "g", and "h".

The ductility of the SC system showed similar changes but the absolute

values are larger than those of the TW system. The lower ductility of the TW system is understandable. Since the TW boundaries block the movement of stacking faults and interfere with the homogeneity or continuity of the applied stress leading to the formation of more defect clusters, stress concentrations are enhanced in the TW system. Thus, under the same loading condition, failure would occur earlier in the TW system due to higher local stress or stress concentrations. The above arguments may be seen in the configurations of the systems at the failure points (see Fig.4.9). As illustrated, failure initiated at random locations near the end of SC system, while in the TW system failure generally initiated at the twin boundaries, indicating that there should be higher stress concentrations at the twin boundaries which facilitate the initiation of failure.

The increment of the ductility with increasing the strain range could be explained as that a larger reversed stress could facilitate pinned defects to escape or the stacking faults to shrink. It should be pointed out that the reversed stress can also generate new defects. However, since it may take more energy to generate new defects than shrink the stacking faults, bearing mind that the shrinkage of stacking faults is accompanied with a decrease in the stacking fault energy. However, for the information on detailed processes related this phenomenon, more studies are needed.

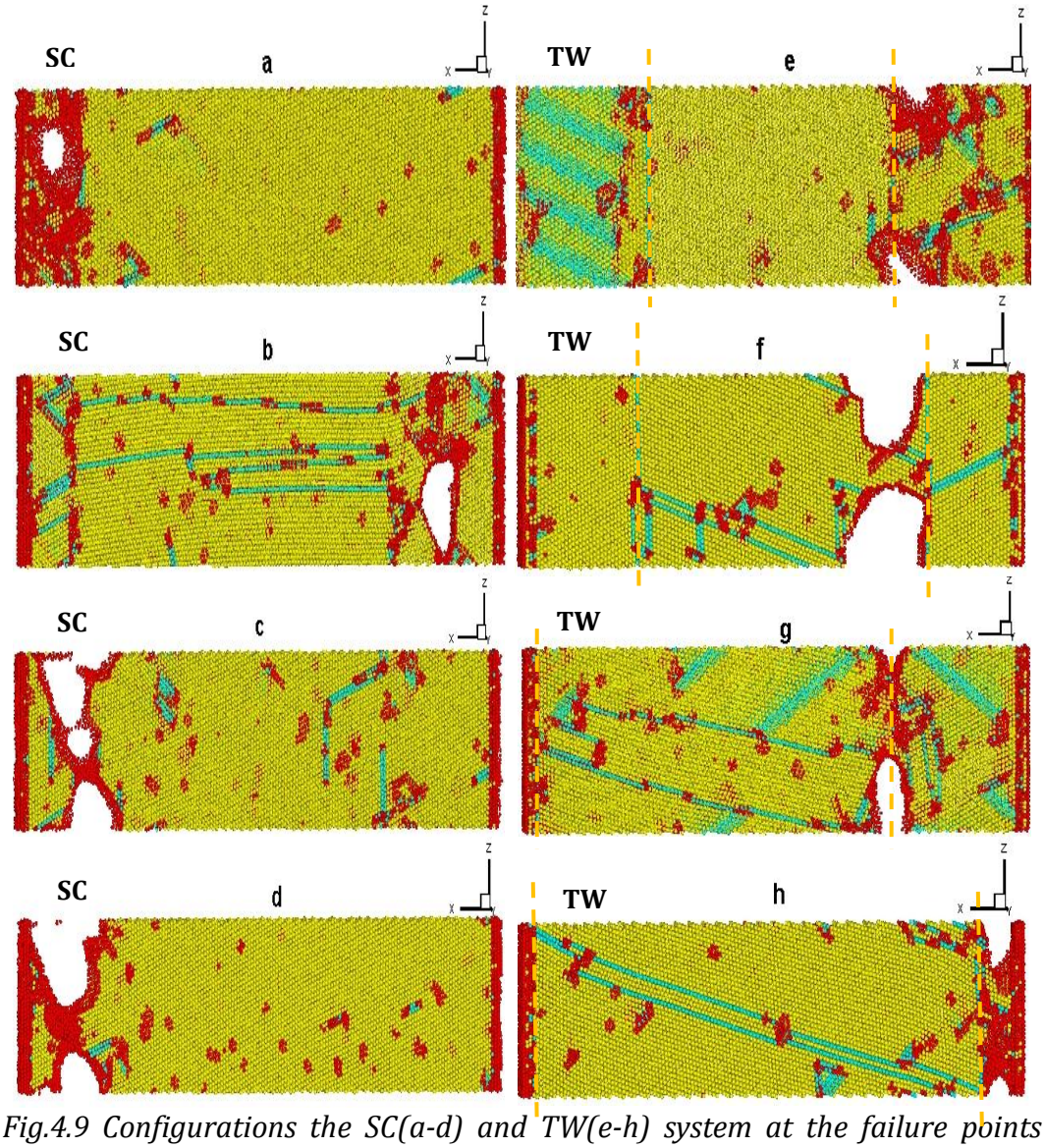

Fig.4.9 Configurations the SC(a-d) and TW(e-h) system at the failure points corresponding to those marked on σ-ε curves shown in Fig.9 (i.e. a, b, c, d, e, f, g and h). Red atoms present the zones near two fixed ends of the model systems and also those with vacancies; blue atoms represent the twin boundaries and generated dislocations and stacking faults, and the yellow atoms display FCC atoms in the model (Note: Initial twin boundaries are marked with dash lines and all the figures are adjusted to approximately the same size for composition. The real length of deformed samples, respectively for SC and TW, increased with increasing the plastic deformation strain as indicated in Fig.4.8, and the twin boundary has shifted.).

4.3 Strain energy and defect quantities

Any deformation process results in corresponding changes in strain energy of a system. It is worth looking at changes in strain energy of the TW and SC systems under the same cyclic loading conditions for better understanding the effect of the TW boundaries on Bauschinger's effect. The system's energy was calculated using the equation, $U = \int_{-|\varepsilon_{tc}|}^{+|\varepsilon_{tc}|} (\sigma_{xx\_tension} - \sigma_{xx\_compression}) d\varepsilon$, for each tension-compression cycle. Here $|\varepsilon_{tc}|$ equals to 10%, 15% and 20%, respectively, for the TW and SC systems; and U represents the total system's energy absorbed in each cycle. Fig.4.10 illustrates the energies of TW and SC systems at the ends of different cycles. As shown, the TW system had a higher energy than the SC system under the same cyclic loading condition, indicating that the TW had high residual stress or the stress relaxation was less easy in the TW system than in the SC system. This suggests that the stress build-up was higher in the TW system due to the presence of the TW boundaries and formation of more defect clusters, which helped to block or pin defects and thus raise local stress with elevated strain-hardening. These are consistent with the observed lower ductility or failure strain of the TW system as shown in Fig.4.8 and its higher failure stress as demonstrated in Fig.4.1.

(a)

(b)

(c)

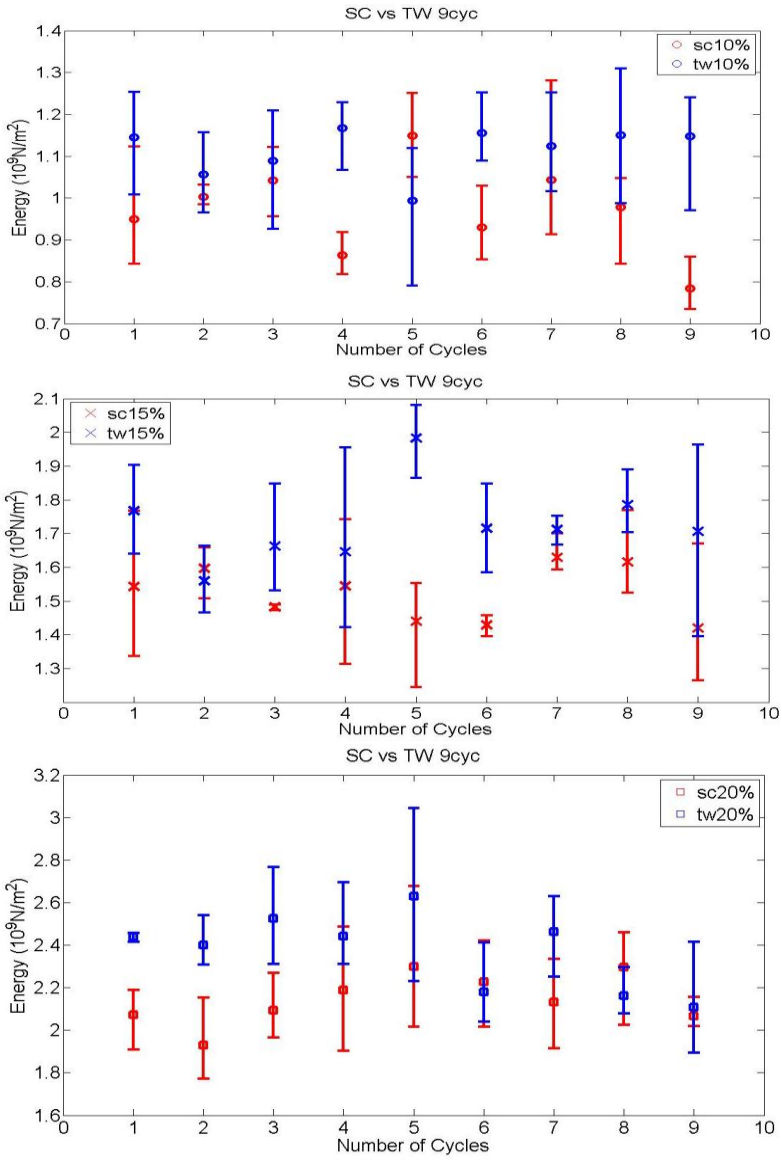

Fig.4.10 The energy absorbed during tension-compression loading cycles with the strain ranges equal to (a) ± 10%, (b) ± 15% and (c) ± 20%, respectively for SC and TW system.

The system's energy results from the existence of defect and its value is dependent on the defect amount and type. Variations in total defect amount of the TW and SC systems were calculated. Fig.4.11 illustrates variations in total defect amount of the TW and SC systems during 1st, 5th and 9th cycles. Since

the deformation started with tension, the defect amount increased during the pulling process while decreased during subsequent compression. This is an indication of the reversible defect movement and annihilation, corresponding to the Bauschinger's effect. Comparing the TW and SC systems, although their defect number – strain curves are different, there is no characteristic difference in the variation of defect amount between the TW and SC systems. Furthermore, on average their total defect quantities are at similar level. Thus, one may expect that the TW system may have more defects of the same type (e.g., dislocations with the same sign) with higher accumulated stress than the SC system, since the energy absorbed in TW is higher than that of the SC as shown in Fig.4.10. This should be attributed to the fact that the TW boundaries block the defect movement and thus have more defects of the same sign accumulated or piled up in front the TW boundaries. The consequently increased stress concentrations may lead to higher stored strain energy (Fig.4.10) and smaller failure strain (Fig.4.8), compared to those of the SC system.

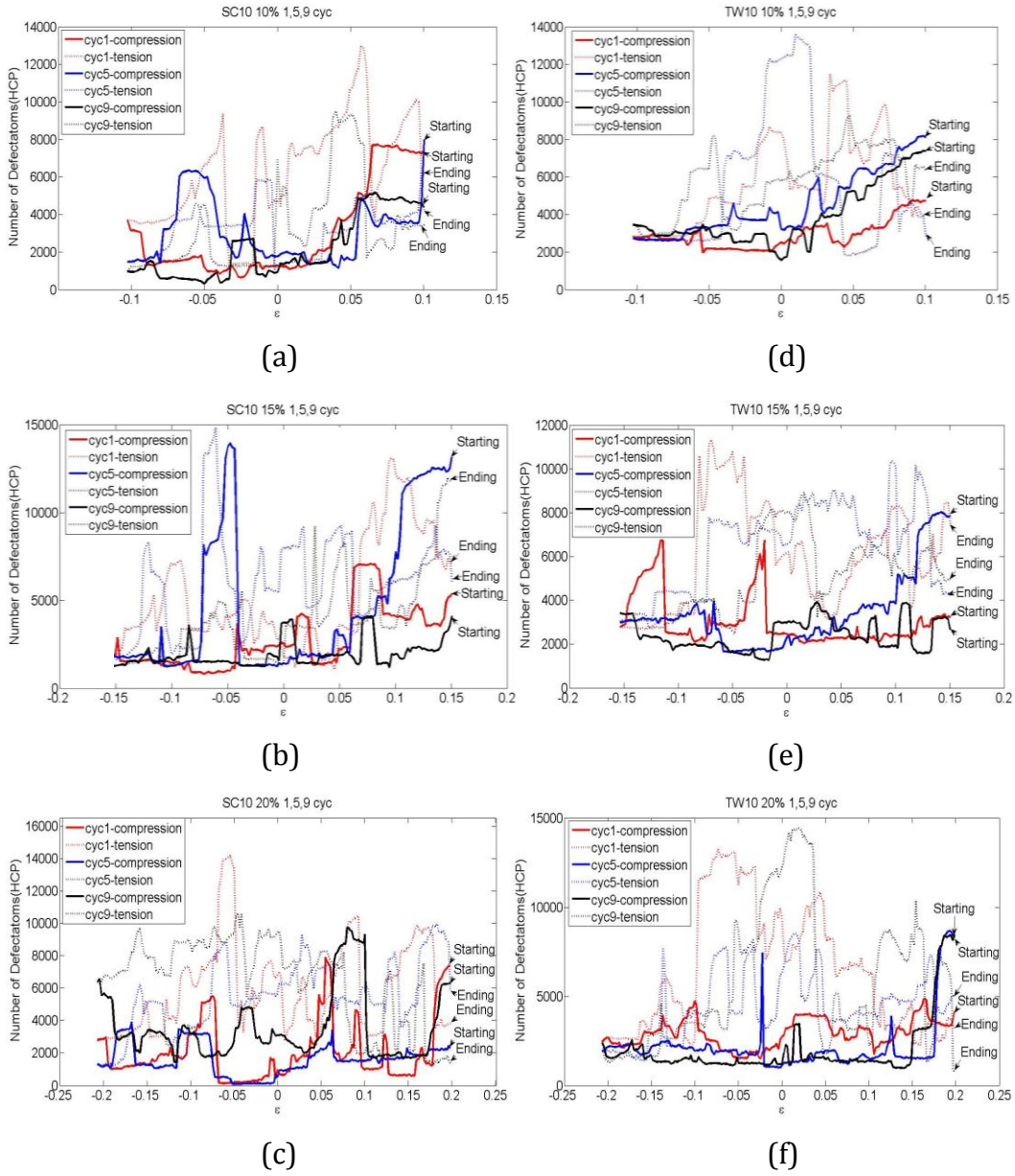

Fig.4.11 Variations in the number of atoms associated with defects during 1st, 5th and 9th tension-compression cycles in the strain ranges equal to ±10% and ±15%, respectively: (a) SC with the strain range of ±10%, (b) SC with the strain range of ±15%, (c) SC with the strain range of ±20%, (d) TW with the strain range of ±10%, (e) TW with the strain range of ±15%, and (f) TW with the strain range of ±20%.

4.4 Summary

A molecular dynamics simulation study was conducted to investigate the effect of twin boundaries on the response of nano-scaled copper systems to tension-compression cyclic loading in the strain ranges of $\pm 10\%$, $\pm 15\%$ and $\pm 20\%$, respectively. Particular attention was put on Bauschinger's effect and relevant issues. The following conclusions are drawn:

(1) Bauschinger's effect existed in nano-scaled copper system with twin boundaries but it was less profound compared to that in single crystal. Such a phenomenon is different from the situation of coarse grain materials, in which twin boundaries may strengthen the Bauschinger's effect. The nano-twin boundaries and formation of more defect clusters suppressed the reversible defect movement and stacking fault shrinkage/extension, which could be responsible for the weaker Bauschinger's effect in the TW system.

(2) The failure strain or ductility of both the SC and TW systems increased with the tension-compression loading cycles. The increase in the failure strain of the TW system was lower than that of the SC system. This could be ascribed to the blocking effect of the TW boundaries, which lowered the reversibility of defects and consequently raised the stress concentrations when the system was under applied stress. These

not only weakened the Bauschinger's effect but also led to lower failure strain for the TW system.

(3) The strain energy of the TW system was higher than that of the SC one, but there was no characteristic difference in the variation of defect quantities between the TW and SC systems and on average their total defect amount were at similar level. Thus, the TW system could have more pile-up of same or similar type defects in front of TW boundaries with higher accumulated local stress, compared to the SC system.

Chapter 5 Effects of grain boundaries in nanocrystalline Cu on its Bauschinger's effect

In this chapter, the influence of grain boundaries on the mechanical behavior and Bauschinger's effect in nanocrystalline copper (GB) during cyclic loading, in comparison with those of Cu single crystal (SC) and Cu with nano-scaled twin boundaries (TW), was computationally investigated employing the molecular dynamics simulation technique. For comparison purpose, some relevant results of SC and TW are represented in this chapter. It was shown that Bauschinger's effect in the systems gradually weakened in the following order: SC, GB and TW. It appears that the annihilation of dislocations or partial dislocations with opposite signs and the shrinkage/extension of associated stacking faults upon stress reversal could be more responsible for the Bauchinger's effect in the nano-copper systems. The cyclic loading process increased the failure strain of the GB, TW and SC systems. However, the increase in the failure strain was less profound in the GB and TW systems. Possible mechanisms responsible for these observations are discussed.

5.1 Bauschinger's Effect in GB, TW & SC nano-systems

5.1.1 The strength of Bauschinger's effect

Cyclic tension-compression deformation processes in the three different systems denoted as GB, SC and TW at a loading rate of $10^7 s^{-1}$ within three maximum strain ranges, ± 10%, ± 15% and ± 20%, respectively, were simulated at room temperature. Cyclic stress-strain curves of the systems within the strain range of ±10% are illustrated in Figure 5.1.

As shown, during the first pulling process, the Cu systems started to yield at the stress between 10 and 15GPa, while during the following cycles, the systems yielded at much lower stress levels (tensile processes) when the stress was reversed from compression to tension, confirming the Bauschinger's effect. The flow stress or yield stress in the subsequent compressive process was also lower than that in the previous tension process. The Bauschinger's effect in copper should result from the cancellation of dislocations with opposite signs as well as the backward movement of partial dislocations and associated stacking fault shrinkage or extension when the applied stress is reversed.

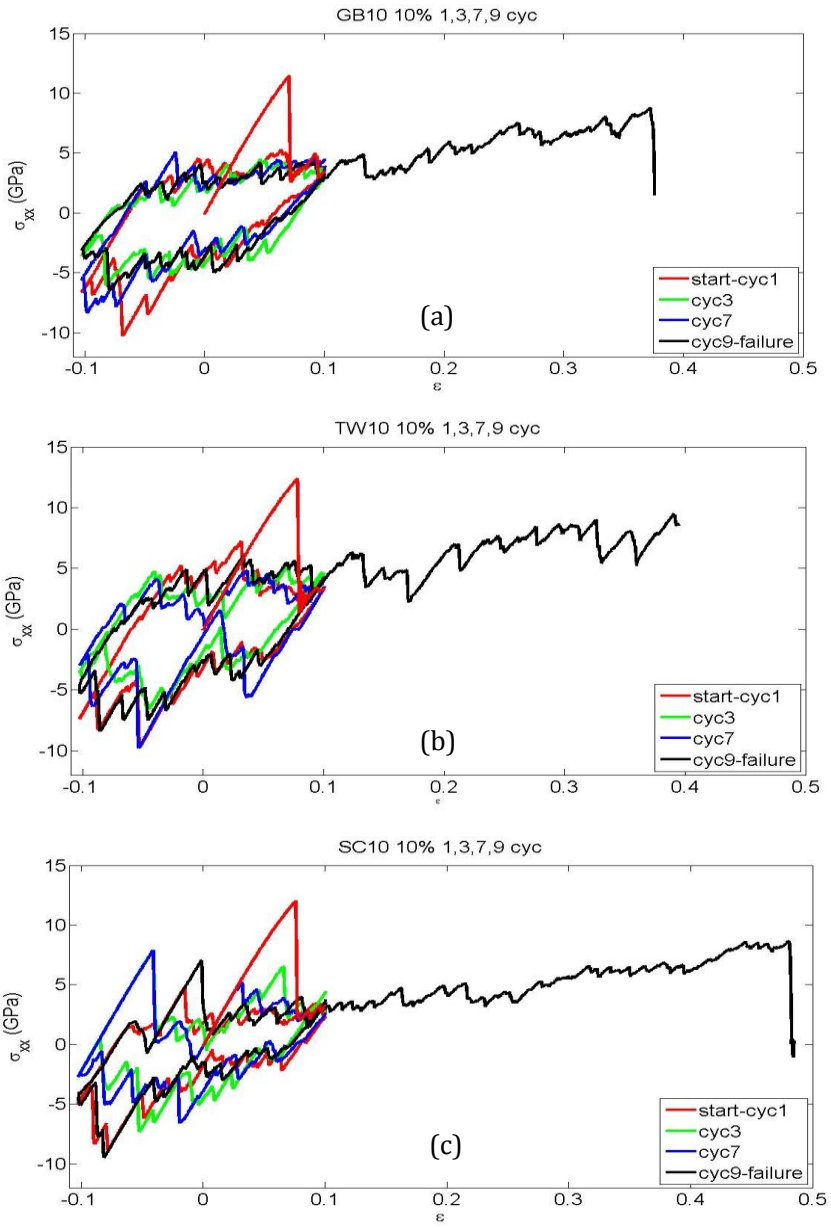

Fig.5.1 σ-ε curves of 1st, 3rd,7th,9th cycles and fracture after nine tensile-compress cycles in the strain range of ±10%: (a) GB system; (b) TW system; (c) SC system.

The system with grain boundaries showed the smoothest stress-strain curves, compared to those of the TW and SC systems. Easier emission of

dislocations from the disordered grain boundaries under the applied stress could be a main responsible factor. It is less easy for dislocations to be emitted from ordered twin boundaries. In the SC system, the generation of dislocations in the crystal lattice, dislocation nucleation at existing dislocations and unpinning of tangled dislocations could also be less easy than the emission of dislocations from grain boundaries, which may thus lead to the roughest stress-strain curves of the SC system. The above explanation is consistent with the mean stress levels of the systems. As shown in Fig.5.1, the mean applied stress for deforming the GB system is lower than those for the TW and SC systems due to the easy emission of dislocations from the grain boundaries. As a result, the smaller barriers to dislocation generation or emission in the GB system should render its stress-strain curves relatively smooth.

In order to have a better insight into the effect of grain boundaries, in comparison with that of twin boundaries, on the Bauschinger's effect in nano-scale copper crystals, the strength of Bauschinger's effect is quantified by using a parameter named B-asymmetry as already defined in the previous chapter, which is the absolute ratio of the maximum stress before stress reversal to the yielding or flow stress in the subsequent reversed deformation process. The larger the B-asymmetry, the stronger the Bauschinger's effect. If

there is no Bauschinger's effect, the value of B-asymmetry is one. Fig.5.2 shows average B-asymmetries of the GB, TW and SC systems, calculated by averaging their B-asymmetry values for all cycles and strain ranges. As illustrated, overall, the nano-twinned copper shows the lowest degree of Bauschinger's effect, followed by the GB system and the SC system has the strongest Bauschinger's effect.

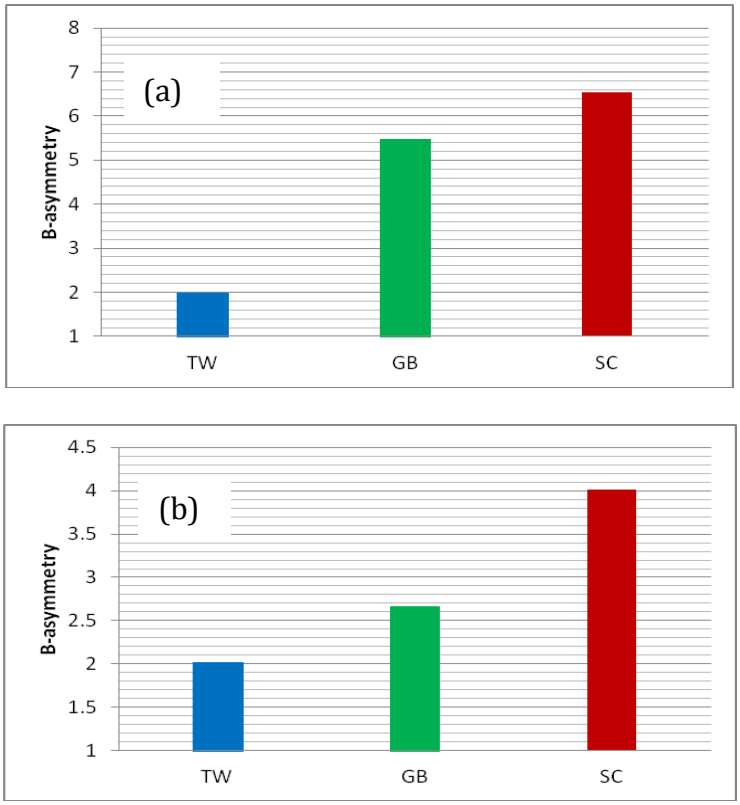

Fig.5.2 Average values of B-asymmetry of the GB, TW and SC systems: (a) B-asymmetry obtained by averaging ratios of the maximum tensile stress to the yielding stress of the subsequent compression of all loading cycles; (b) B-asymmetry obtained by averaging ratios of the maximum compressive stress to the yielding stress of subsequent tensile process of all loading cycles.

It is known that interfaces, such as grain boundaries and twin boundaries, generally enhance the Bauschinger's effect [35, 36, 69], resulting from increased back stress when dislocations pile up in front of the interfaces. However, in the nanocrystalline crystals, the small spacing between the boundaries may largely limit the defect movement and stacking fault extension or shrinkage, which may weaken the Bauschinger's effect. Our previous studies in chapter 4 showed that in the case of twin boundaries, the backward movement of dislocations appeared to be hindered, since the nano-scaled spacing between the ordered twin boundaries possibly set larger barriers to defects (leading to low freedom of defects) and associated strain energy is high. For the disordered grain boundaries, the situation is different since grain boundaries are active sources of dislocations. Thus in the nanocrystalline materials with a large volume fraction of grain boundaries with small spacing between the boundaries associated with complicated internal stress state, the grain boundaries may not effectively block dislocation movement but could readily absorb and emit dislocations, rendering the GB system to exhibit its Bauschinger's effect stronger than that of the TW system but weaker than that of the SC system as Fig.5.2 illustrates.

It is worth noting that the B-asymmetry values of SC and GB systems during tension-compression reversal (i.e. tension and then compression) are

larger than those during compression-tension reversal, implying that the Bauschinger's effect is stronger in the former process than in the latter. However, this appears not to be applicable to the TW system.

The difference in B-asymmetry between tension-compression and compression- tension may come from the difference in stress for dislocation nucleation between tension and compression in cyclic deformation. By atomistic simulation, Tschopp et al [70, 71] demonstrated that the stresses for both homogeneous dislocation nucleation and that occur at grain boundaries are higher in compression than in tension. Such difference could result from different variations in Burgers vector of the slip plane caused by compression and tension respectively. For a slip system with its normal near 45 degrees relative to the applied uniaxial stress (corresponding to the maximum shear stress), a larger compressive stress is required to activate the slip system than a tensile stress because its component normal to the slip plane expands the atomic spacing on the slip plane, thus increasing the magnitude of Burgers vector and consequently elevating the difficulty for dislocations to nucleate and glide on this slip plane [16]. Based on the above discussion, under a tensile stress, more dislocations could be activated and pile up in front of an obstacle, accompanied with larger local stress or back stress. As the stress is reversed, the applied compressive stress could drive the dislocation pile-ups move

backwards more easily than generate new dislocations. The situation could be different for a compression-tension stress reversal process, during which dislocation pile-ups could be less with lower back stress during the compression process and more new dislocations could be generated during subsequent tensile process. As a result, the stress relaxation and backward movement of defects during tension-compression reversal could be easier, corresponding to a stronger Bauschinger's effect.

The above mechanism for the difference in the strength of the Bauschinger's effect may not be applicable to the TW nano-system. Unlike the single crystal or grain boundary that is a source and also a sink of dislocations, where dislocations are relatively easier to be generated or emitted, the ordered twin boundaries in nano-scaled systems may more confine dislocations and their higher interfacial stresses could mutually influenced and also interfere the applied stress. These could be responsible for the minimized difference in Bauschinger's effect between tension-compression and compression-tension processes.

5.1.2 Changes in configurations during stress reversal

For more details about the response of the GB system to cyclic loading in comparison with those of the SC and TW systems, configurations of samples

before and after stress reversal were collected. Fig.5.3 (a) – (c) illustrate σ-ε curves of 3rd & 4th cycles of the three systems within the strain range of ±20%. The points around the maximum tensile strain at the end of 3rd cycle are marked with "a1", "b1" & "c1" for the three systems, respectively. "a2", "b2" and "c2" are points at which the stress was reduced to zero. The yielding points during subsequent compressive deformation of the three systems are marked with "a3", "b3" & "c3", respectively. Configurations corresponding to these points are also presented in Fig.5.3. Similar points at the other end of the stress-strain curves for the compression-tension stress reversal and corresponding configurations are also marked and presented in Fig.5.3.

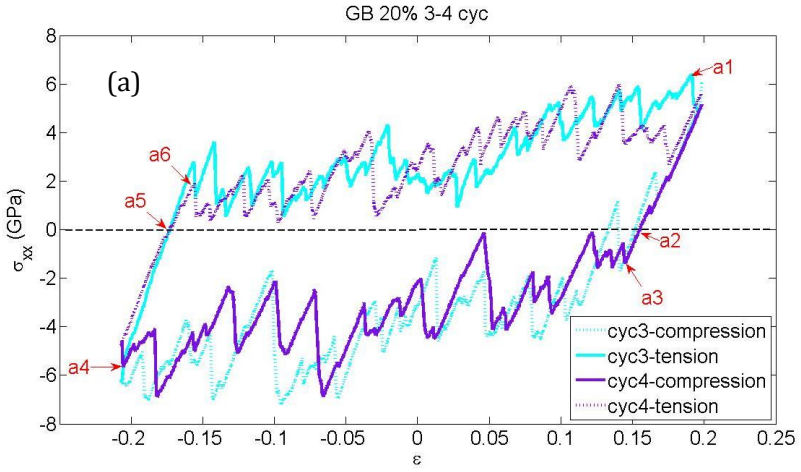

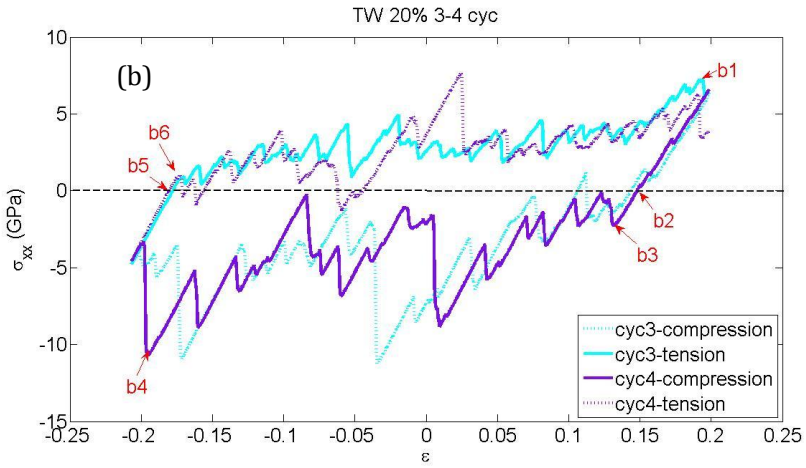
TW 20% 3-4 cyc
(b)
b1
b2
b3
b4
b5
b6
cyc3-compression
cyc3-tension
cyc4-compression
cyc4-tension
σxx (GPa)
ε

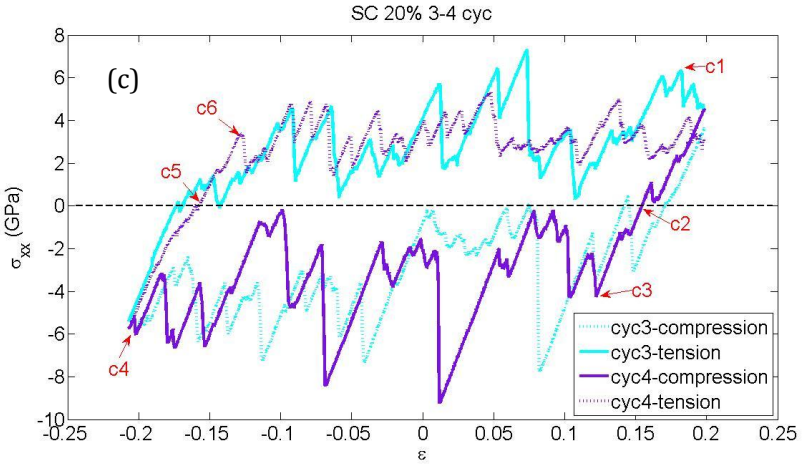
SC 20% 3-4 cyc
(c)
c1
c2
c3
c4
c5
c6
cyc3-compression
cyc3-tension
cyc4-compression
cyc4-tension
σxx (GPa)
ε

GB

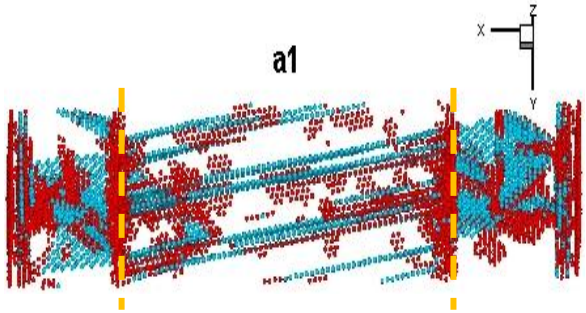
a1
X
Z
Y

GB

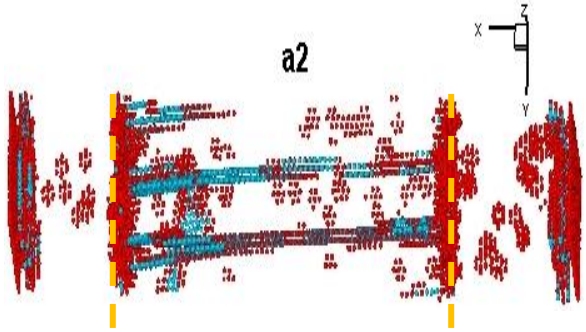
a2
X
Z
Y

GB

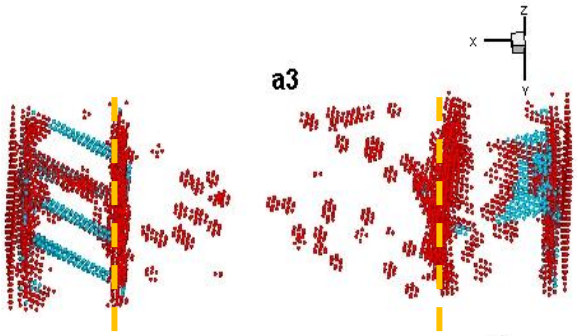

GB

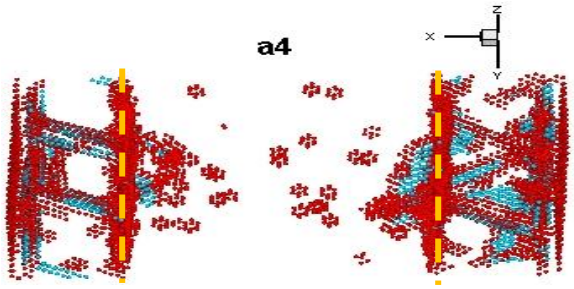

GB

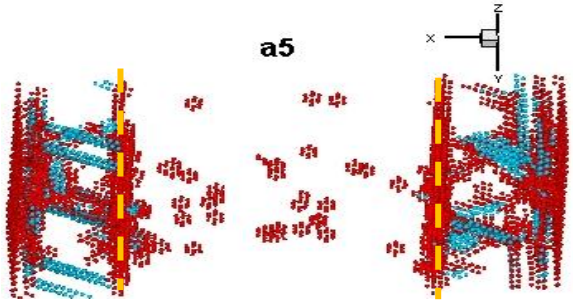

GB

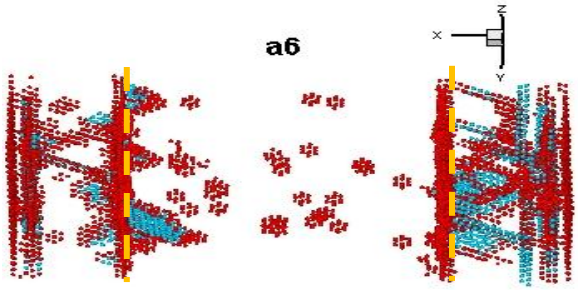

TW

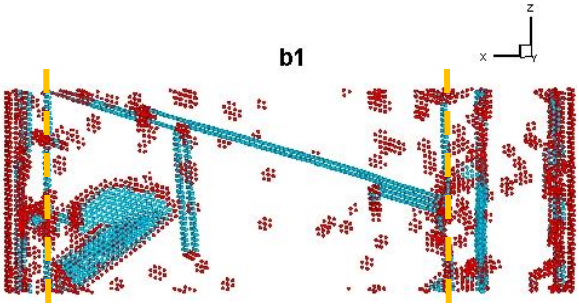

TW

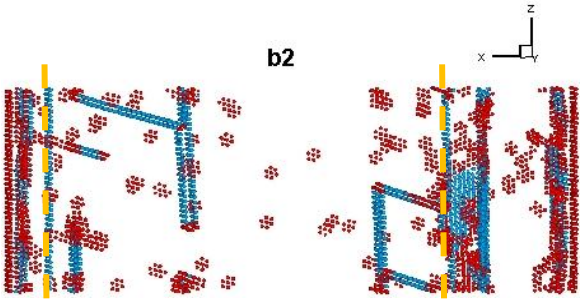

TW

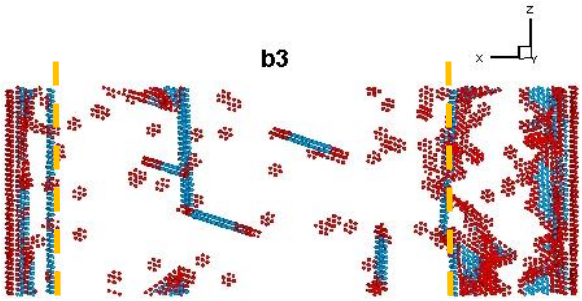

TW

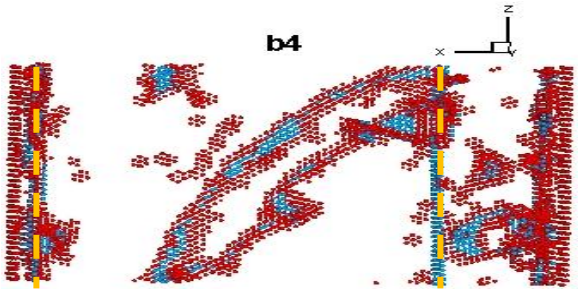

TW

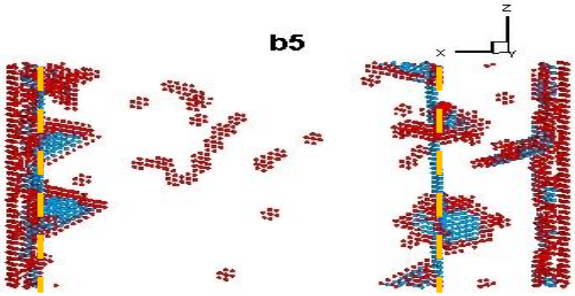

TW

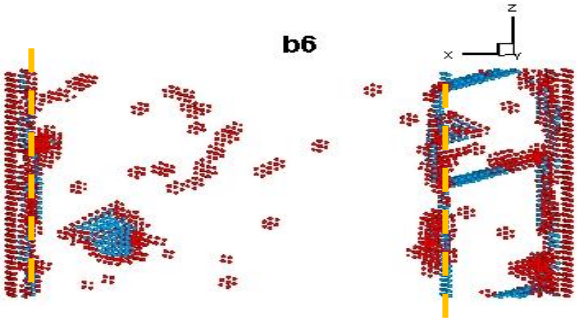

SC

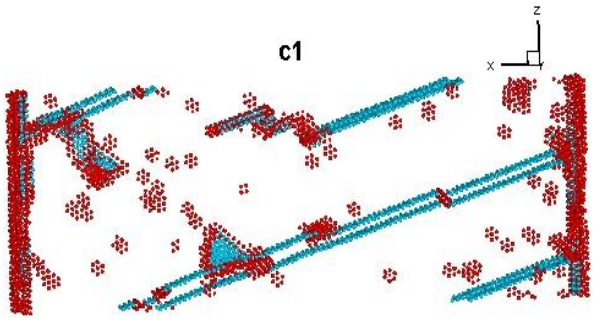

SC

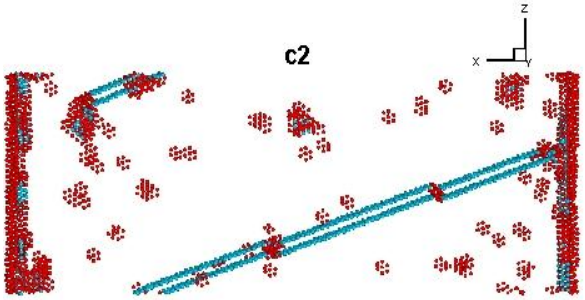

SC

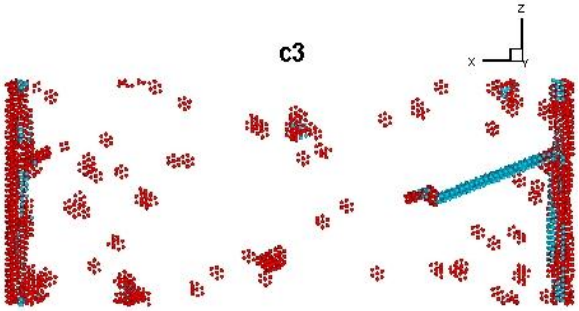

SC

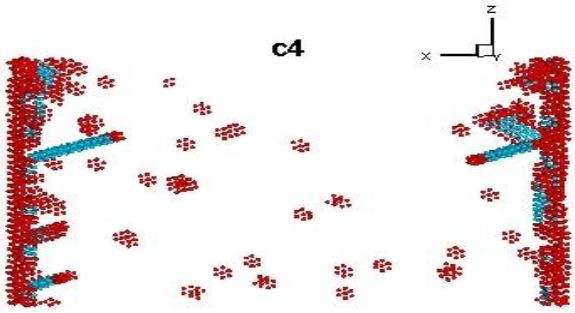

SC

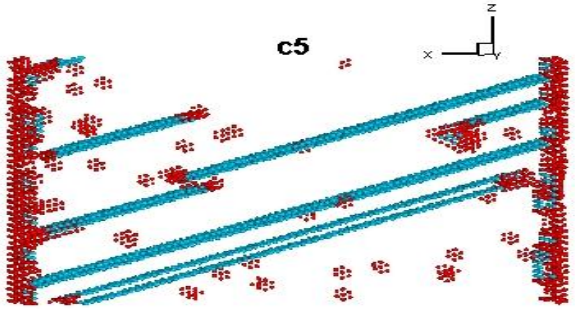

SC

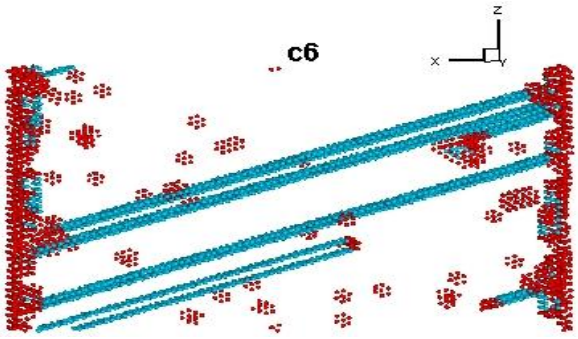

Fig.5.3 (a)–(c) σ-ε curves of 3rd & 4th cycles of the three systems within the strain range of ± 20%. Configurations of marked points around ends of the σ-ε curves in (a)–(c) corresponding to stress reversal respectively in the GB(a1-a6), TW(b1-b6) and SC(c1-c6) system are illustrated. Blue areas represent stacking faults and TW boundaries, and red domains represent grain boundaries, other defects such as vacancies and dislocations, and the fixed end layers of the systems. Initial twin boundaries and grain boundaries are marked with yellow dash lines.

As shown, at point a1 quite a large portion of the GB system is occupied by the stacking faults, which shrink during stress release (a2) and reversal (a3), showing the reversibility of the stacking faults, though the grain boundaries still block the stacking faults. However, the stacking fault is much less in the TW system and other defects appear little reversible during stress release and reversal (see the configurations of b1, b2 and b3). Or in other words, in the TW system the shrink and regeneration of stacking faults is less profound, and the annihilation of defects with opposite signs could be more constrained by the twin boundaries in the nano-scaled TW system. The SC system behaves similarly to the GB system (see configurations of c1, c2 and c3)

but the stacking faults can expand or shrink through the entire system, implying higher reversibility of the stacking faults. In the GB system, although grain boundaries may block the partial dislocation movement, the grain boundaries can absorb and emit dislocations easily, leading to enhanced annihilation of defects with opposite signs and shrinkage or extension of stacking faults. These could explain why Bauschinger's effect is weaker in the TW system, compared to the GB and SC systems. The observed changes in configuration are consistent with the trend of B-asymmetry for the three systems i.e. B-asymmetry (SC)> B-asymmetry (GB)> B-asymmetry (TW).

The configurations at the other end of σ-ε curves are consistent with the lowered B-asymmetry during compression-tension stress reversal, compared to that of tension-compression stress reversal, as shown in Fig.5.2. The systems show less defect pile-ups (at points of a4, b4 and c4) and, except that of the TW system, the configurations do not change much when the applied stress is released (a5 and b5) and reversed (a6 and b6). This could be an indication of lower defect reversibility during the compression-tension stress reversal process, corresponding to weaker Bauschinger's effect. For the SC system, stacking faults are generated during the stress reversal process, corresponding to stronger Bauschinger's effect, compared to the GB and TW systems.

5.1.3 Stored strain energy

When the defect reversibility is lower and the annihilation of defects with opposite sign is less easy, the internal strain energy built during the loading cycles could be higher. The internal energy fluctuations during the loading cycles for the three systems were analyzed. The internal energy for each cycle was calculated using the equation:

$$U = \int_{-|\varepsilon_{tc}|}^{+|\varepsilon_{tc}|} (\sigma_{xx\_tension} - \sigma_{xx\_compression}) d\varepsilon,$$

where $|\varepsilon_{tc}|$ is equaled to 10%, 15% and 20%, respectively for different loading conditions; U represents the system's total strain energy absorbed during each cycle. Results of the calculation are illustrated in Fig.5.4, which demonstrates that the energies of the GB and SC systems are similar and lower than that of the TW system. This internal energy analysis gives results that are consistent with the argument that the defect reversibility in the TW system is lower.

Based on Fig.5.1 and Fig.5.4, the lower flow or yield stresses level, relatively smooth stress-strain curves, and lower absorbed energy in the GB system may imply that grain boundaries in the nano-scaled system could reversibly accommodate deformation with ease through defect emission and absorption without large built-up internal strain and stored energy, compared to the TW system. As for the SC system, no internal obstacles (interfaces and second phases) are present, which makes the system more reversible during loading

cycles, showing higher Bauschinger's effect and low stored strain energy.

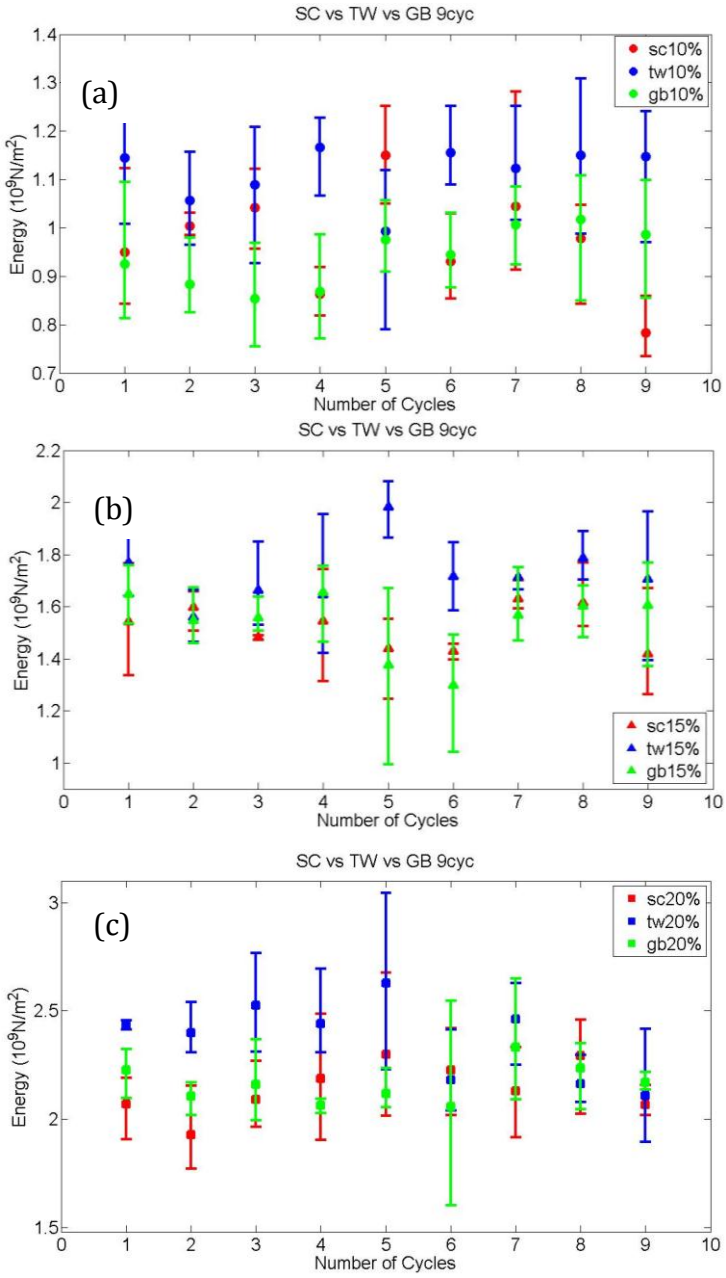

Fig.5.4 Energy absorption in the GB, TW and SC systems during loading cycles within different strain ranges: (a) ± 10%, (b) ± 15%, and (c) ± 20%.

5.2 Main factors that contribute to the Bauschinger's effect in the nano-systems

Bauschinger's effect could result from two factors:

1) The reversible movement of dislocations from places where dislocations pile up with higher stress concentrations; when the applied stress is reversed, the piled-up dislocations may move backwards at a lower applied stress level since the previously built internal back stress helps drive the backward movement of the defects.
2) Annihilation of dislocations when new dislocations with opposite sign are generated by reversed applied stress. The annihilation of dislocations with opposite signs leads to minimization of strain energy and is thus an energy-favorable process.

Both the above factors may result in softening during stress reversal. However, the second factor could play a more important role in the nano-systems, based on the argument that if the first factor is predominant, then we may expect that the TW system could have stronger Bauschinger's effect, since the ordered twin boundaries may more effectively block dislocations with larger local back stress that favors the backward movement of dislocations piled up in front of the twin boundaries before stress reversal.

However, this expected phenomenon was not revealed by the simulation. Instead, the TW system shows the weakest Bauschinger's effect. As discussed earlier, the backward movement of dislocations could be hindered because of nano-scaled spacing between the twin boundaries which set larger barriers to defects and limit their freedom with associated high strain energy.

Thus, the annihilation of dislocations or partial dislocations with opposite signs and the shrinkage of associated stacking faults could become more important for the Bauchinger's effect in the nano-systems. As indicated earlier, the GB system showed stronger Bauschinger's effect, compared to the TW system. The easier emission of dislocations with opposite sign from grain boundaries as the stress is reversed may enhance the dislocation annihilation and thus Bauschinger's effect. We determined the variations in defect quantities during a tension-compression cycle, which showed profound defect annihilation. Fig.5.5 illustrates variations in the total numbers of generated HCP defects during 2^{nd}, 4^{th} and 6^{th} cycles in the strain ranges of $\pm$ 10%, 15% and $\pm$ 20%, respectively. As shown, the defect number increased during tension and considerably decreased during the following compression process. The defect annihilation appeared somewhat stronger in the GB and SC systems, compared to that in the TW system, since the difference in the number of defect atoms between tension and compression

processes is relatively smaller for the TW system.

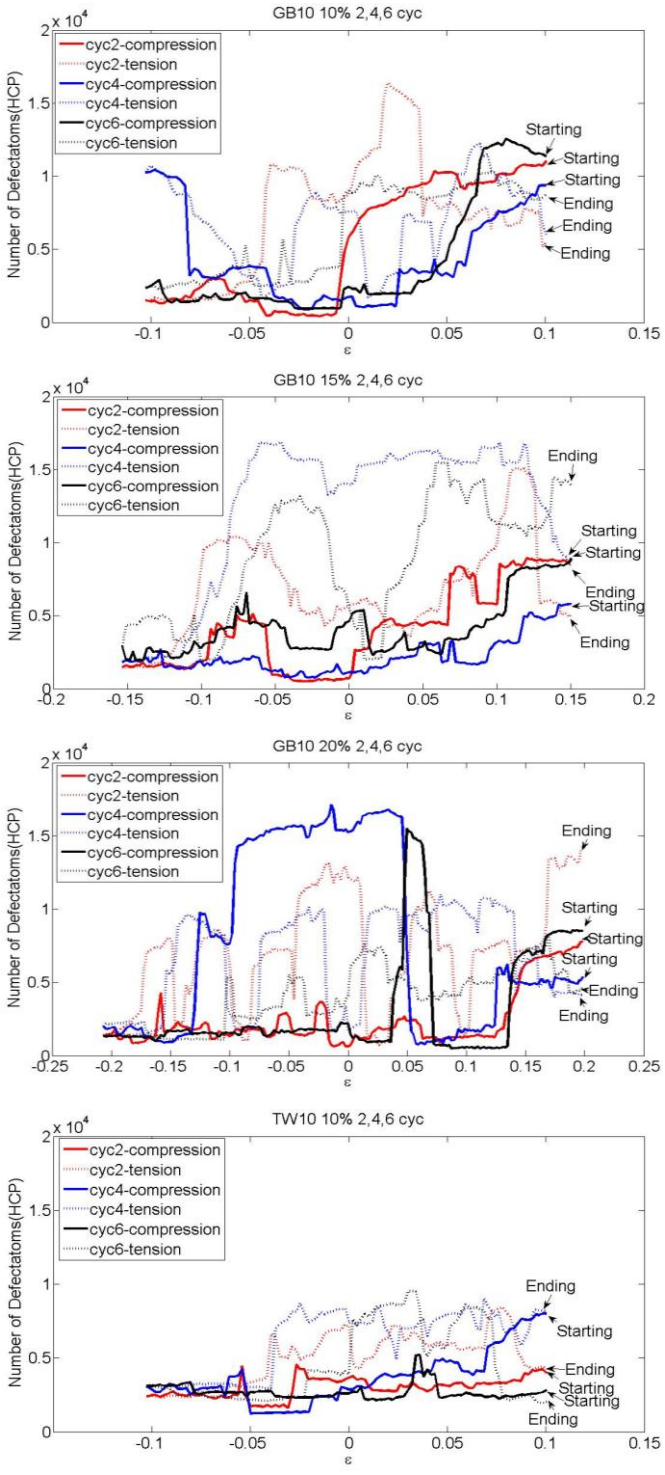

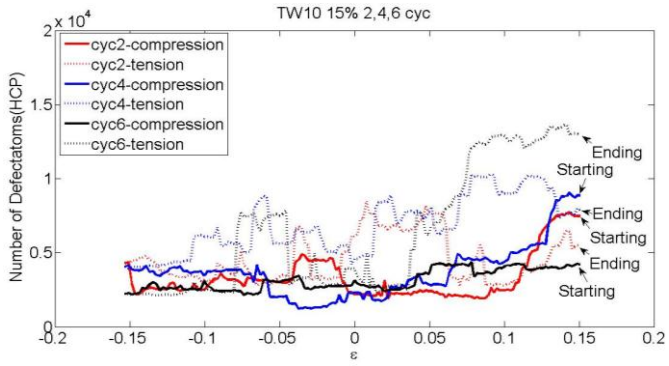
TW10 15% 2,4,6 cyc
x 10^4
cyc2-compression
cyc2-tension
cyc4-compression
cyc4-tension
cyc6-compression
cyc6-tension
Number of Defectatoms(HCP)
ε
Ending
Starting
Ending
Starting
Ending
Starting

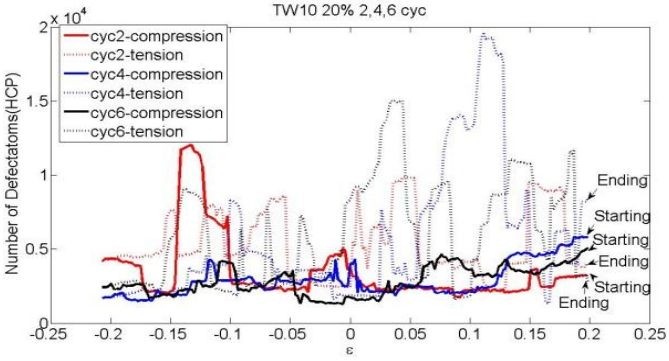
TW10 20% 2,4,6 cyc
x 10^4
cyc2-compression
cyc2-tension
cyc4-compression
cyc4-tension
cyc6-compression
cyc6-tension
Number of Defectatoms(HCP)
ε
Ending
Starting
Starting
Ending
Starting
Ending

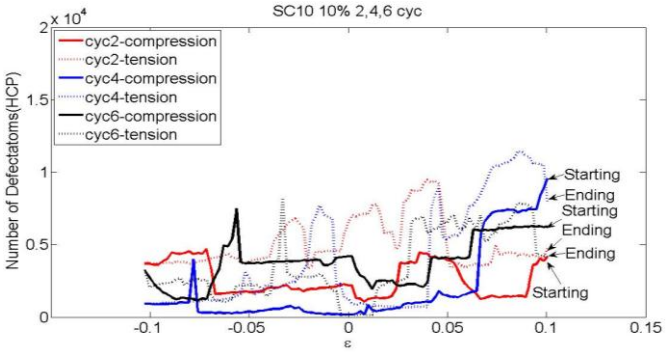
SC10 10% 2,4,6 cyc
x 10^4
cyc2-compression
cyc2-tension
cyc4-compression
cyc4-tension
cyc6-compression
cyc6-tension
Number of Defectatoms(HCP)
ε
Starting
Ending
Starting
Ending
Ending
Starting

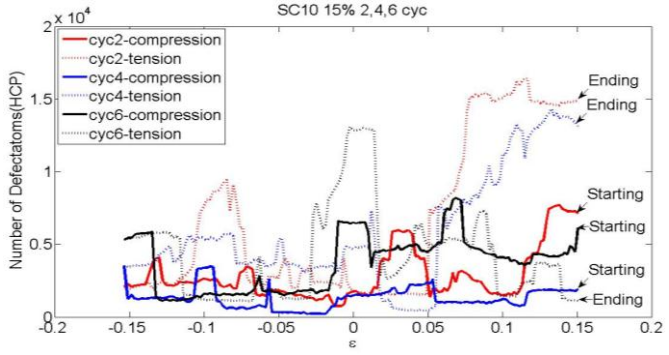
SC10 15% 2,4,6 cyc
x 10^4
cyc2-compression
cyc2-tension
cyc4-compression
cyc4-tension
cyc6-compression
cyc6-tension
Number of Defectatoms(HCP)
ε
Ending
Ending
Starting
Starting
Starting
Ending

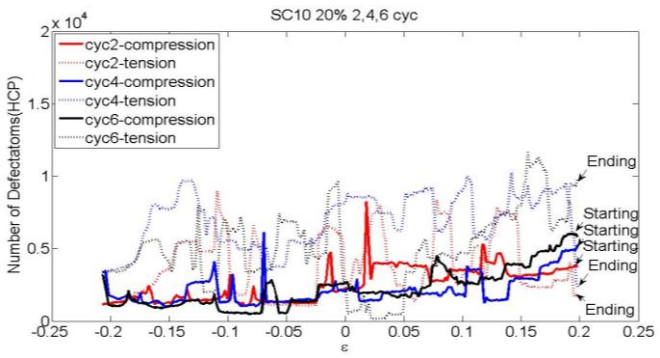

Fig.5.5 Variations in the number of defect atoms during 2nd, 4th and 6th loading cycles for the GB, TW and SC systems in different strain ranges.

5.3 Failure strain

The influence of grain boundaries on the fracture strain of nano-sized copper crystal after cyclic tensile-compressive deformation was investigated in comparison with that of a single crystal and one of twin boundaries. The failure strain has been defined in chapter three (see section 3.2.3).

The failure strains of the SC, TW and GB systems under different cyclic loading conditions were determined. Up-to-failure σ-ε curves of all the systems are illustrated in Fig.5.6, where the failure points are alphabetically marked from "a" to "l". Corresponding engineering elongation and true elongation in the GB system are listed in Table 5.1.

Compared to the SC system and the TW system, the failure strain increased for all the systems under all cyclic loading conditions. The increase in the failure strain by the stress cycling is explainable. For an annealed

sample, failure will occur when similar dislocations having the same signs accumulate to reach a certain level (generated local stress reaches the tensile strength) under unidirectional loading. However, for a sample experienced cyclic loading, e.g., nine cycles in the present case, the dislocations generated during a previous loading process would cancel some of new dislocations with opposite signs generated by the reversed stress during the subsequent pulling process up to failure. This could help reduce the build-up of stress, leading to an increase in the failure strain or ductility.

The increase in the failure strain is less profound in the GB and TW systems as shown in Fig.5.6. This should be attributed to the fact that grain boundary and twin boundary more or less block the dislocation movement and stacking fault extension or shrinkage, resulting in higher stress at the boundaries to promote failure. Configurations at the failure points marked by letters from “a” to “l” in Fig.5.6 are presented in Fig.5.7 and corresponding stress distributions right before fracture are illustrated in Fig.5.8, respectively.

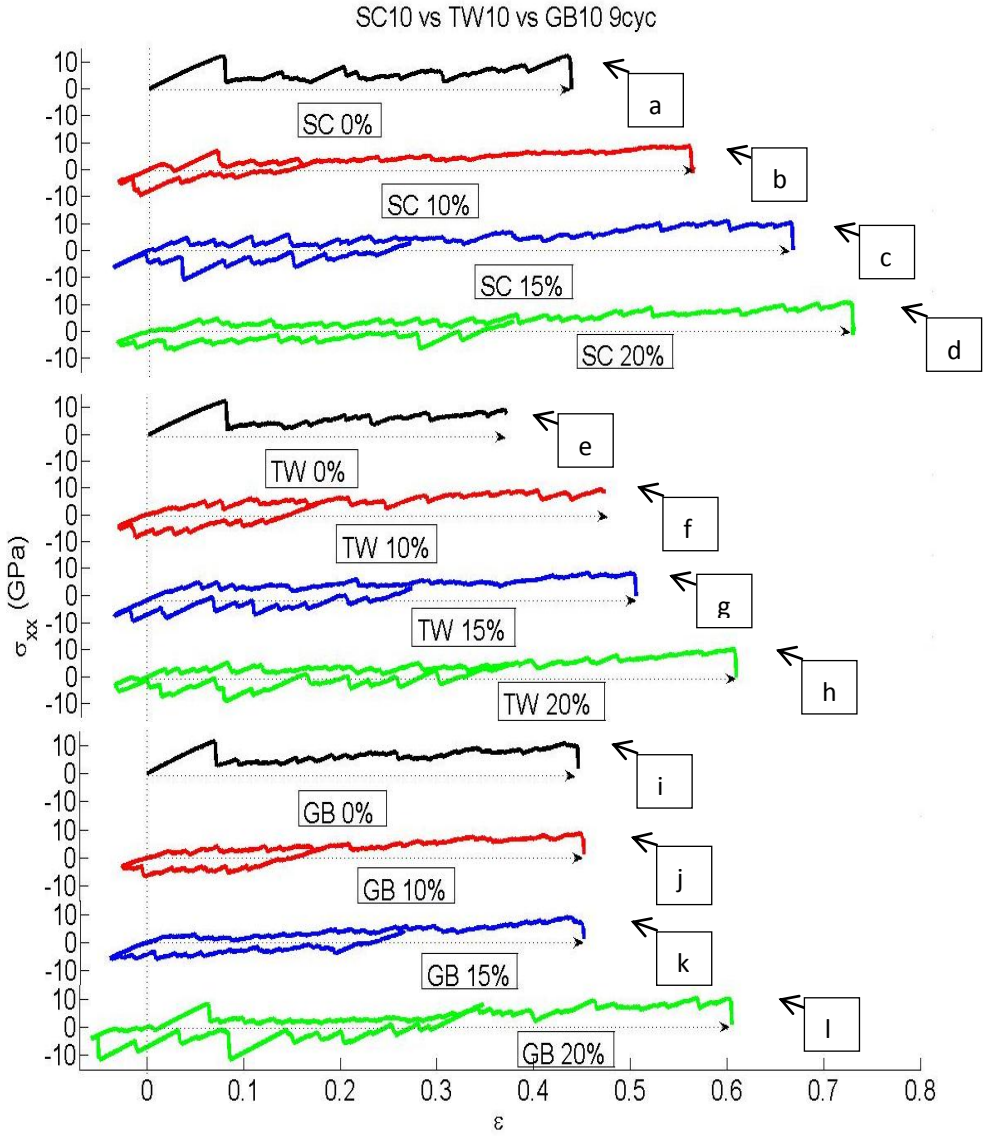

Fig.5.6 Up-to-failure σ-ε curves of SC, TW & GB samples cyclically loading in different strain ranges: 0%, ±10%, ±15% and ±20. Failure points after deformation for all systems are alphabetically marked from "a" to "l".

Table 5.1 - Failure strains of the GB system experiencing single-pulling and nine stress cycles with plastic strain=10%, 15% and 20%

System	ε	X_1	X_2	$\%EL_{engineering}$	$\%EL_{true}$
Grain Boundary	singlepulling	0	0.4452	44.52%	36.83%
	±10%	-0.07637	0.3739	48.75%	39.71%
	±15%	-0.1143	0.3353	50.76%	41.05%
	±20%	-0.1495	0.4548	71.05%	53.68%

SC

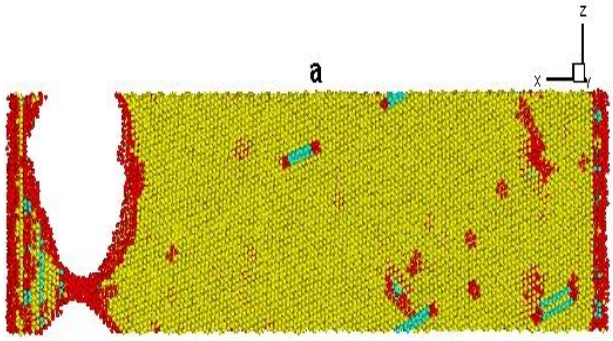

SC

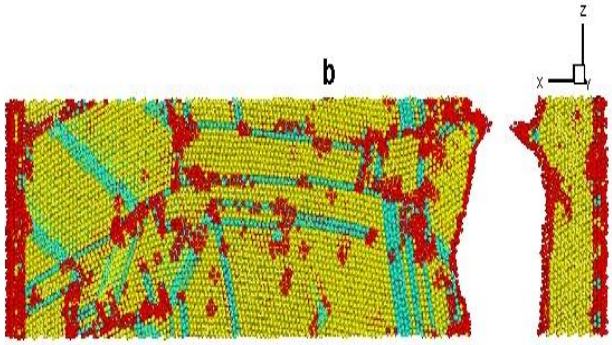

SC

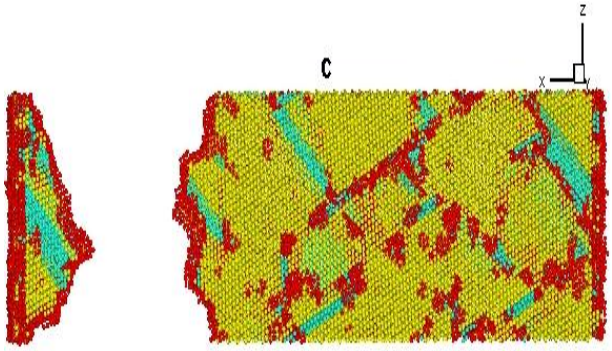

SC

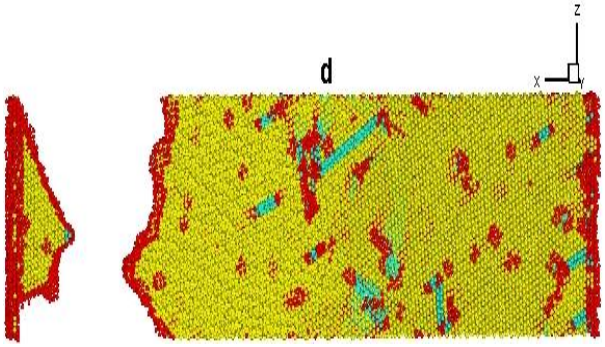

TW

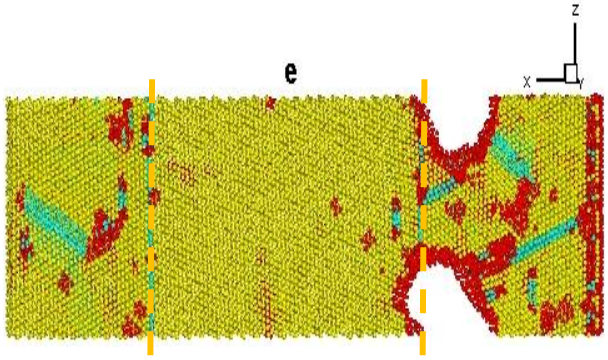

TW

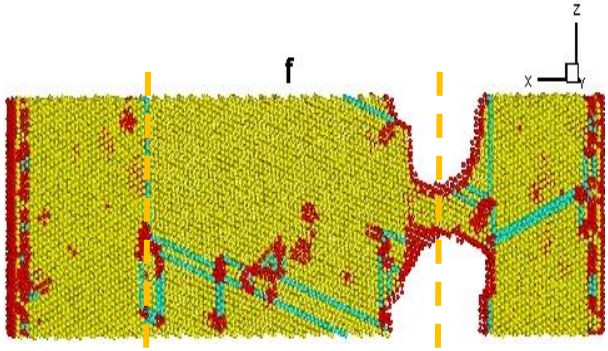

TW

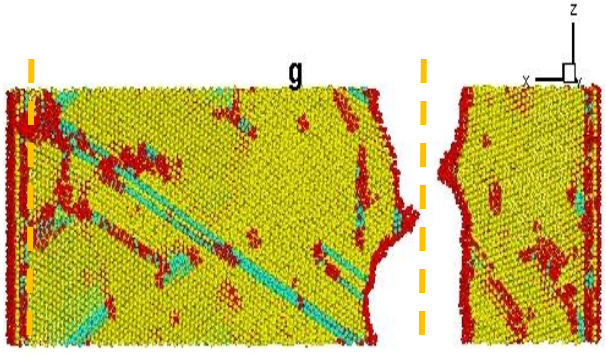

TW

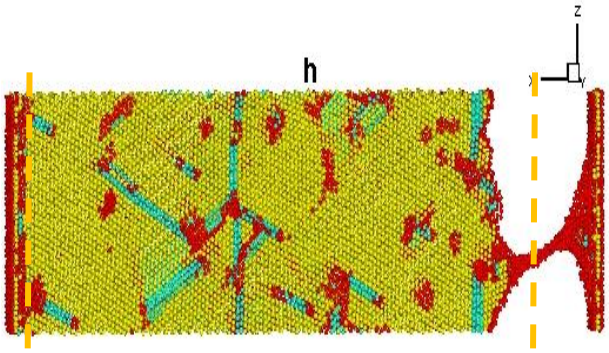

GB

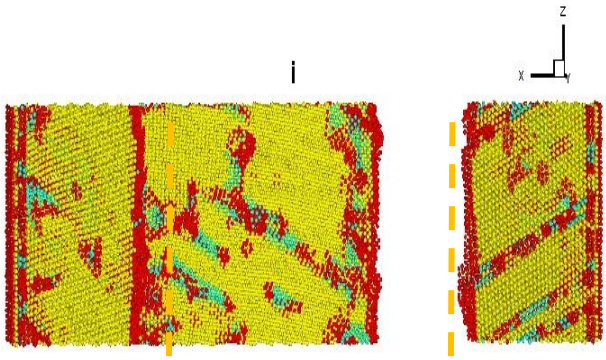

GB

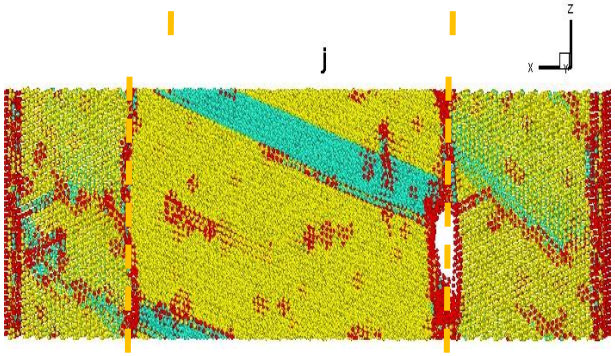

GB

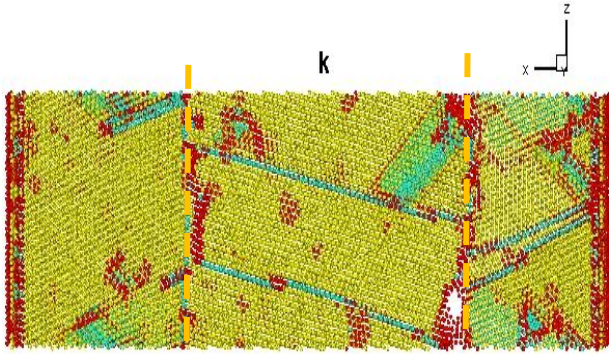

GB

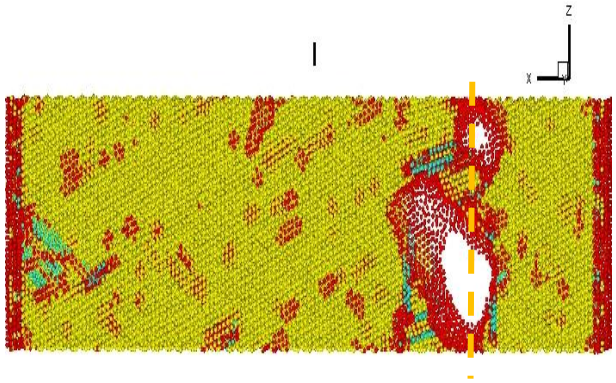

Fig.5.7 Configurations of the SC(a-d), TW(e-h) & GB(i-l) systems at the failure points corresponding to those marked at σ-ε curves shown in Fig.5.6 (i.e. a, b, c, d, e, f, g, h, i, j, k & l). Blue areas represent stacking faults and TW boundaries, red domains represent grain boundaries and clusters of vacancies as well as atoms in the fixed end layers at the ends of the systems. Initial twin boundaries and grain boundaries are marked with yellow dash lines. (Note: The figures of fractured samples were adjusted to approximately the same size.).

As shown in Fig.5.7, fracture occurred near the end of the SC system due to the edge effect, while in the GB and TW systems fracture occurred at grain boundaries and twin boundaries, respectively, at which the extension of stacking faults were blocked. When the defect movement is blocked, the local stress is raised, which promotes the initiation of fracture. The higher local stresses or stress concentrations near the boundaries have been shown in Fig.5.8.

The stress distributions shown in Fig.5.8 are consistent with the failure strains of the different systems as indicated in Fig.5.6. When the stress concentration level of a system is higher, fracture occurs earlier in the system. The higher stress concentrations at the TW and GB boundaries should be

responsible for lower failure strains or ductility.

SC

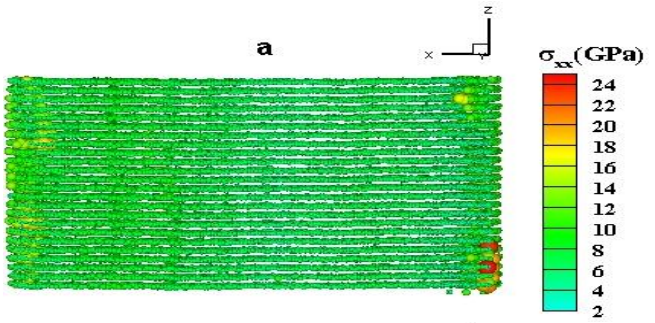

SC

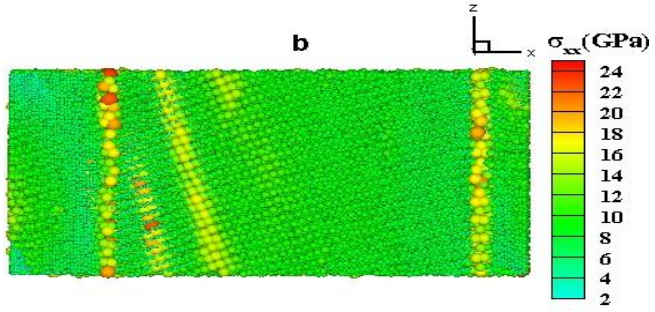

SC

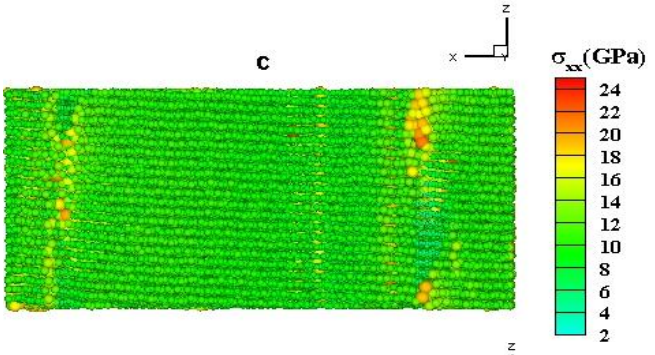

SC

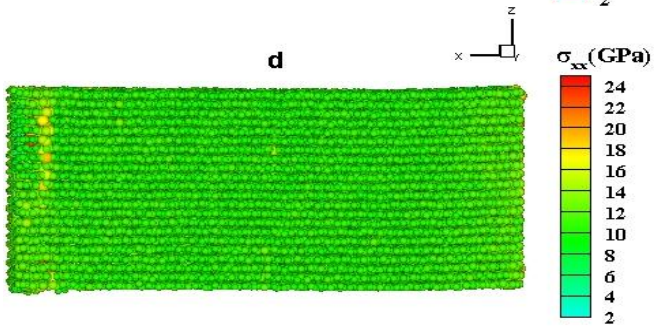

TW

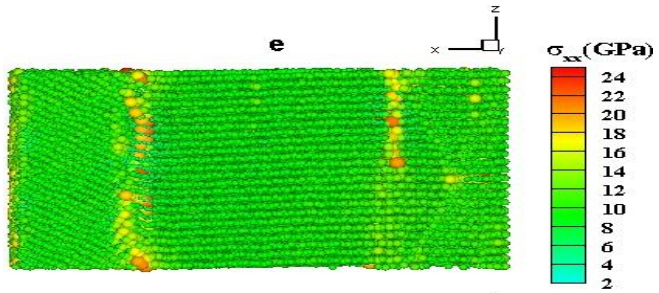
e
z
x
σxx(GPa)
24
22
20
18
16
14
12
10
8
6
4
2

TW

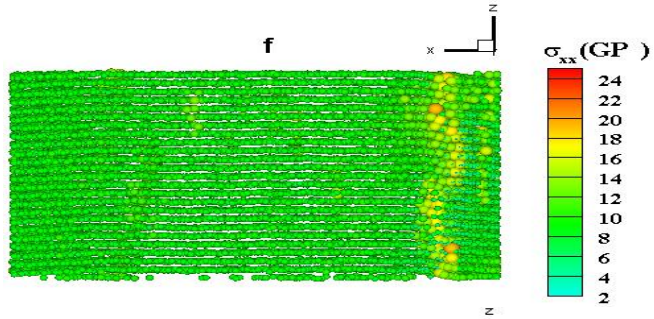
f
z
x
σxx(GP)
24
22
20
18
16
14
12
10
8
6
4
2

TW

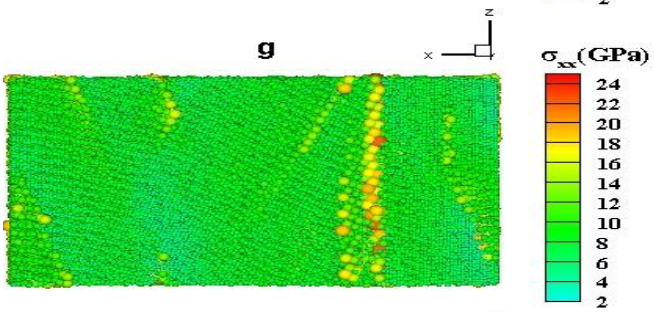
g
z
x
σxx(GPa)
24
22
20
18
16
14
12
10
8
6
4
2

TW

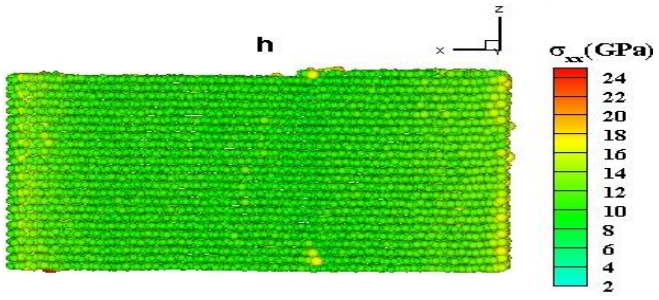
h
z
x
σxx(GPa)
24
22
20
18
16
14
12
10
8
6
4
2

GB

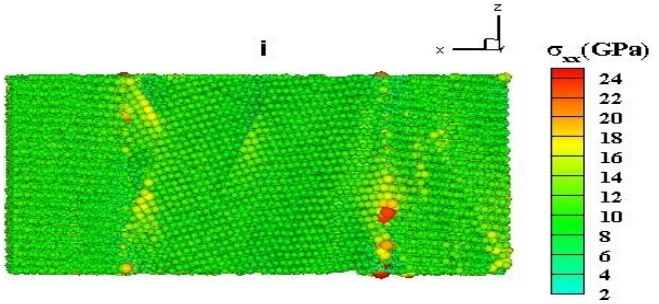
i
z
x
σxx(GPa)
24
22
20
18
16
14
12
10
8
6
4
2

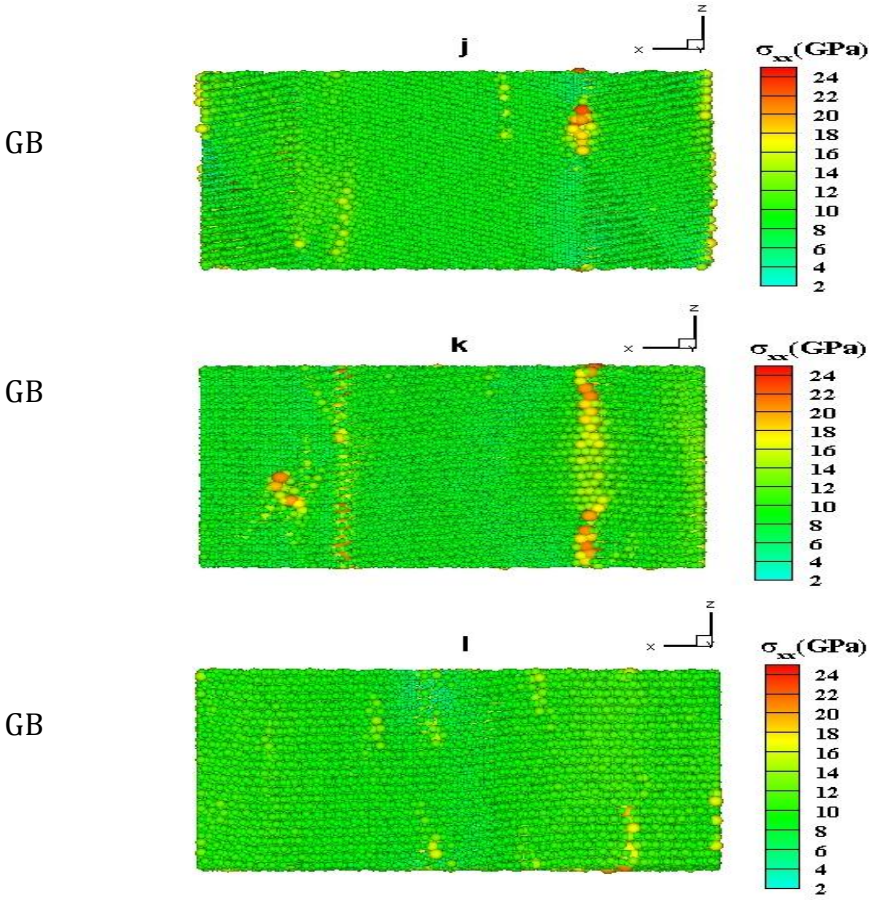

Fig.5.8 Stress concentrations in the three Cu systems, i.e. the SC(a-d), TW(e-h) & GB(i-l) systems, prior to fracture at the points marked in Fig.5.6. Magnitude of local stress (σ_{xx}) is represented by color.

It is interesting to notice that the stress concentrations in the systems are lowered or the stress distribution becomes less heterogeneous after experienced cyclic loading in the strain range of $\pm 20\%$ (see Fig.5.8 d, h, l), compared to those in the systems experienced cyclic loading in smaller strain ranges. A possible mechanism responsible for such a phenomenon is that the

defect backward movement and cancellation of dislocations with opposite signs could be enhanced as the magnitude of deformation is increased, which may also be seen from the changes in defect quantities during loading cycling in different strain ranges (Fig.5.5). As shown in Fig.5.5, the defect densities at the end of compression process of loading cycles become lower with an increase in the strain range, implying that the systems may bear more deformation when pulled to failure. Besides, larger strain-range loading cycling could also modify the configurations of grain boundaries and twin boundaries (e.g., deteriorate the degree of interfacial ordering) to minimize the stress concentration at the boundaries. These may lower the build-up of local internal stress or reduce the stress homogeneity, which could be the reason why the failure strain increases with the increase in the strain range of deformation cycling as shown in Fig.5.6.

5.4. Summary

Employing the molecular dynamics simulation method using the LAMMPS software, the influence of grain boundaries in nano-scaled Cu crystal (GB) on its mechanical behavior was investigated, with emphasis on the Baushinger's effect during cyclic tensile-compressive deformation processes within strain ranges of ± 10%, ± 15% and ± 20%, respectively. Results were compared to

those of single crystal (SC) and twinned (TW) systems on nano-scale for comprehensive understanding. The following conclusions are drawn:

(1) Bauschinger's effect exists in the GB system, which is stronger than the Bauschinger's effect in the TW system but weaker than that in the SC system. Compared to the ordered twin boundaries, grain boundaries have the capability of emitting and absorbing dislocations, which more facilitates the cancellation of dislocations with opposite signs during the cyclic loading processes, leading to stronger Bauschinger's effect. The single crystal without structure obstacles, however, shows the strongest Bauschinger's effect. It should be indicated that the above conclusions may not be applicable to microcrystalline or polycrystalline systems in which defects have much larger free space to move within grains.

(2) In the nano-systems, the strain energy introduced in the GB system by cyclic loading is lower than that in the TW system and slightly higher than that of the SC system, which is an indication that the apparent "reversibility" of defects in the nano-scaled GB system is comparable to that in the SC system due to the capability of GB in emitting and absorbing dislocations. While the ordered twin boundaries in a nano-scaled system show stronger confinement to defects.

(3) It appears that in the nano-scaled systems the annihilation of dislocations or partial dislocations with opposite signs and the shrinkage of associated stacking faults could be more responsible for the Bauchinger's effect, since the limited spacing between grain boundaries, particularly twin boundaries, confine reversible or backward movement of dislocations from places where dislocations pile up with higher local stress concentrations.

(4) The cyclic loading process increased the failure strain of the GB, TW and SC systems, which is related to the Bauschinger's effect. The increase in the failure strain is less profound in the GB and TW systems, which could be attributed to the fact that both the grain and twin boundaries can more or less block the dislocation movement and stacking fault extension, resulting in higher stress concentrations at the boundaries to promote failure.

Chapter 6 Suggested follow-up studies

In all three nano-scale copper systems, including single crystalline, crystalline with two coherent Σ3 twin boundaries and one embedded two Σ7 grain boundaries, the failure strain increased after cyclic tension-compression straining. The failure strain also increased with the increment of deformation strain range, though less profound in the TW and GB system compared to that in the SC system. The phenomena were understood, since the reversal of applied stress may facilitate the backward motion and subsequent cancellation of existing partial dislocations with opposite signs, which helped to relax the stress concentration in the systems. However, increasing strain range also meant larger portions of the material will be destroyed, which can create new defects with similar types and they can interact and tangle with existing partial dislocations, consequently elevating the stress level and resulting in early fracture. Thus, which of these two processes affect in the deformation with increasing strain ranges and how the stress concentration would change with the strain range, more effort are needed in order to obtain detailed information.

Migrations of boundaries after cycling were observed and are illustrated in Fig.5.8. However, how the microstructure of boundaries accommodated with the generation of partial dislocations and how they gradually moved to the

new places or disappeared during the deformation, details are needed. We may track the trajectories of the atoms that consisted of the boundaries in future work. Such information is helpful to further understand the role of grain boundaries in a nano-scale system.

Three layers of atoms in two ends of the system were fixed. Although their effects could be ignored in our comparison with different systems, the fixed region may more or less influence the response of the nano-scale systems to cyclic loading, e.g., blocking the movement of generated partial dislocations and other type of defects, causing stress concentrations that lead to fracture. These could be further studied in order to understand better the intrinsic mechanical behavior of nano-scaled systems.

Bibliography

[1] R. Sowerby, D.K. Uko. Mater Sci Eng A 1979;41:43.

[2] T.S. Srivatsan, Meslet Al-Hajri, J.D. Troxell. Mech Mater 2004;36: 99.

[3] J.B. Jordon, M.F. Horstemeyer, K. Solanki, Y. Xue. Mech Mater 2007;39:920.

[4] C.Y. Tang, D.Y. Li, G.W. Wen. Tribol Lett 2010;41:569.

[5] O.B. Pedersen, L.M. Brown, W.M. Stobbs. Acta Mater 1981;29:1843.

[6] M. Haouaoui, I. Karaman, H.J. Maier. Acta Mater 2006;54:5477.

[7] C. Tang, J.M. Wang, G.W. Wen, Y. Wang, D.Y. Li. Wear 2011;271:1237.

[8] L. Yue, H. Zhang, D.Y. Li. Scripta Mater 2010;63:1116.

[9] G.P. Potirniche, M.F. Horstemeyer, B. Jelinek, G.J. Wagner. Int J Fatigue 2005;27:1179.

[10] K.J. Zhao, L.L. Fan, C.Q. Chen. Acta Mech Solida Sin 2009;22:650.

[11] K.J. Zhao, C.Q. Chen, Y.P. Shen, T.J. Lu. Comp Mater Sci 2009;46:749.

[12] M. Buciumeanu, L. Palaghian, A.S. Miranda, F.S. Silva. Int J Fatigue 2011;33: 145.

[13] J.H. Yang, Y. Li, S.X. Li, C.X. Ma, G.Y. Li. Mater Sci Eng A 2001;299:51.

[14] P.J. Guruprasad, W.J. Carter, A.A. Benzerga. Acta Mater 2008;56:5477.

[15] S. Queyreau, B. Devincre. Philo Mag Lett 2009;89:419.

[16] D.Y. Li. Phys Status Solidi A 2002;191:427.

[17] P. Lukas, L. Kunz, M. Svoboda. Mater Sci Eng A 1999;272:31.

[18] D. Kiener, C. Motz, W. Grosinger, D. Weygand, R. Pippan. Scripta Mater 2010;63: 500.

[19] N. Chawla, B. Jester, D.T. Vonk: Mater Sci Eng A 2003;346:266.

[20] E. Demir, D. Raabe. Acta Mater 2010;58:6055.

[21] R.E. Stoltz, R.M. Pelloux. Metall Mater Trans A 1976;7:1076.

[22] G.D. Moan, J.D. Embury. Acta Mater 1978;27:903.

[23] P.S. Bate, D.V. Wilson. Acta Mater 1986;34:1097.

[24] A.R. Setoodeh, H. Attariani: Mater Lett 2008; 62:4266.

[25] R. HSU, R.J. Arsenault. Mater Sci Eng 1984;66:35.

[26] A.S. Argon. Strengthening mechanisms in plasticity, 1st ed. Oxford: Oxford University Press; 2008.

[27] F. Prinz, A.S. Argon. Phys Status Solidi A 1980;57:741.

[28] T. Rzychoñ, K. Rodak. Arch Mater Sci Eng 2007;28:605.

[29] C.J. Shute, B.D. Myers, S. Xie, T.W. Barbee Jr., A.M. Hodge, J.R. Weertman. Scripta Mater 2009; 60:1073.

[30] K. Lu, L. Lu, S. Suresh. Science 2009;324:349.

[31] M. Dao, L. Lu, Y.F. Shen, S. Suresh. Acta Mater 2006;54:5421.

[32] H. Mirkhani, S.P. Joshi. Acta Mater 2011;59:5603.

[33] I. Shabib, R.E. Miller. Modeling Simul Mater Sci Eng 2009;17:055009.

[34] A. Marchenko, H. Zhang. Metall Mater Trans A 2012;43:3547.

[35] M.G. Stout, A.D. Rollett: Metall Mater Trans A 1990;21:3201.

[36] I. Karaman, H. Sehitoglu, Y.I. Chumlyakov, H.J. Maier, I.V. Kireeva. Metall Mater Trans A 2001;32:695.

[37] R.J. Asaro. Acta Metall 1975;23:1255.

[38] W.E. Carrington, D. Mclean. Acta Metall 1965;13:493.

[39] H. Margolin, S. Stanescu. Acta Metall 1975;23:1411.

[40] H. Margolin, F. Hazaveh, H. Yaguchi. Scr Metall 1978;12:1141.

[41] H. Yaguchi, H. Margolin. Scr Metall 1980;14:627.

[42] F. Barlat, J.J. Gracio, M.G. Lee, E.F. Rauch, G. Vincze. Int J Fatigue 2011; 27:1309.

[43] J.H. Kim, D.Y. Kim, F. Barlat, M.G. Lee. Mater Sci Eng A 2012;539: 259.

[44] L.L. Li, Z.J. Zhang, P. Zhang, Z.F. Zhang. Scripta Mater 2011;65:505.

[45] M. Yuasa, T. Nakazawa, M. Mabuchi. Mater Sci Eng A 2010;527:2629.

[46] M. Yuasa, T. Nakazawa, M. Mabuchi. Mater Sci Eng A 2010;528:260.

[47] G.P. Potirniche, M.F. Horstemeyer, B. Jelinek, G.J. Wagner. Int J Fatigue 2005;27:1179.

[48] Yu.S. Danilov. Met Sci Heat Treat 1964;6: 563.

[49] H. Yaguchi, H. Margolin. Metall Mater Trans A 1986;17:2017.

[50] E.A. Holm, D.L. Olmsted, S.M. Foiles. Scripta Mater 2010;63:905.

[51] B. Sivaiah, S.P. Gupta. Mater Charact 2008;59:1141.

[52] N. Goukon, T. Ikeda, M. Kajihara. Acta Mater 2000;48:1551.

[53] Z.F. Zhang, Z.G. Wang. Mater Sci Eng A 1999;271:449.

[54] H. Fang, M.F. Horstemeyer, M.I. Baskes, K. Solanki, Comput Methods Appl Mech Engrg 2004; 193:1789.

[55] A. Vinogradov, Y. Kaneko, K. Kitagawa, S. Hashimoto, V. Stolyarov, R. Valiev. Scripta Mater, 1997;36:1345.

[56] V.L. Tagarielli, N.A. Fleck, A. Colella, and P. Matteazzi. J Mater Sci 2011;46: 385.

[57] L. Yue, H. Zhang, D.Y. Li. Acta Mater 2010;58:2677.

[58] D. Frenkel, B. Smit. Understanding Molecular Simulation: From Algorithms to Applicaitons, 2nd ed. London: Academic Press;2002.

[59] S. Nose. Mol Phys 1984;52:255.

[60] W.G. Hoover. Phys Rev A 1985;31:1695.

[61] S.M. Foiles, M.I. Baskes, M.S. Daw. Phys Rev B 1986;33:7983.

[62] Y. Mishin, M.J. Mehl, D.A. Papaconstantopoulos, A.F. Voter, J.D. Kress. Phys Rev B 2001;6322:224106.

[63] S. Plimpton. J Comput Phys 1995;117:1.

[64] A.S. Clarke, H. Jonsson. Phys Rev E 1993;47:3975.

[65] T.H. Courtney. Mechanical Behavior of Materials, 2nd ed., Boston: McGraw-Hill Book Co.;2000.

[66] O. Buck, D. Schumacher, A. Seeger. Phys Status Solidi B 1973;60:707.

[67] S.J. Goldberg, R.J. Maciag, K.Mukherjee. Metall Mater Trans B 1970;1: 1079.

[68] P. Ballo, V. Slugen. Comp Mater Sci, 2005;33:491.

[69] O. Ciuca, K. Tsuchiya, Y. Yokoyama, Y. Todaka, M. Umemoto. Mater Trans 2009; 50:1123.

[70] M.A. Tschopp, D.L. McDowell. J Mech Phys Solids 2008;56:1806.

[71] M.A. Tschopp, G.J. Tucker, D.L. McDowell. Comput Mater Sci 2008;44:351.